LIGHT FLICKER EVALUATION OF ELECTRIC ARC FURNACES BASED ON NOVEL SIGNAL PROCESSING ALGORITHMS

A THESIS SUBMITTED TO
THE GRADUATE SCHOOL OF NATURAL AND APPLIED SCIENCES
OF
MIDDLE EAST TECHNICAL UNIVERSITY

BY

NESLİHAN KÖSE

IN PARTIAL FULFILLMENT OF THE REQUIREMENTS
FOR
THE DEGREE OF MASTER OF SCIENCE
IN
ELECTRICAL AND ELECTRONICS ENGINEERING

SEPTEMBER 2009

Approval of the thesis:

LIGHT FLICKER EVALUATION OF ELECTRIC ARC FURNACES BASED ON NOVEL SIGNAL PROCESSING ALGORITHMS

submitted by **NESLİHAN KÖSE** in partial fulfillment of the requirements for the degree of **Master of Science in Electrical and Electronics Engineering Department, Middle East Technical University** by,

Prof. Dr. Canan Özgen
Dean, Graduate School of **Natural and Applied Sciences** ______________

Prof. Dr. İsmet Erkmen
Head of Department, **Electrical and Electronics Engineering** ______________

Prof. Dr. Kemal Leblebicioğlu
Supervisor, **Electrical and Electronics Engineering Department, METU** ______________

Dr. Özgül Salor
Co-supervisor, **TÜBİTAK-UZAY; Electrical and Electronics Engineering Department, Gazi Üniv.** ______________

Examining Committee Members:

Prof. Dr. Muammer Ermiş
Electrical and Electronics Engineering, METU ______________

Prof. Dr. Kemal Leblebicioğlu
Electrical and Electronics Engineering, METU ______________

Assoc. Prof. Dr. Tolga Çiloğlu
Electrical and Electronics Engineering, METU ______________

Prof. Dr. Işık Çadırcı
Electrical and Electronics Engineering, Hacettepe University ______________

Assist. Prof. Dr. Çağatay Candan
Electrical and Electronics Engineering, METU ______________

Date: 10 / 09 / 2009

I hereby declare that all information in this document has been obtained and presented in accordance with academic rules and ethical conduct. I also declare that, as required by these rules and conduct, I have fully cited and referenced all material and results that are not original to this work.

Name, Last Name: NESLİHAN KÖSE

Signature :

ABSTRACT

LIGHT FLICKER EVALUATION OF ELECTRIC ARC FURNACES BASED ON NOVEL SIGNAL PROCESSING ALGORITHMS

Köse, Neslihan

M.S., Department of Electrical and Electronics Engineering

Supervisor : Prof. Dr. Kemal Leblebicioğlu

Co-Supervisor : Dr. Özgül Salor

September 2009, 81 pages

In this research work, two new flickermeters are proposed to estimate the light flicker caused by electric arc furnaces (EAFs) where the system frequency deviates significantly. In these methods, analytical expressions of the instantaneous light flicker sensation are obtained beginning from a voltage waveform and these expressions are used to obtain a flicker estimation method based on the IEC (International Electrotechnical Commission) flickermeter. First method is a spectral decomposition based approach using DFT to estimate the light flicker. The leakage effect of the DFT algorithm due to fundamental frequency variation is reduced by employing spectral amplitude correction procedure around the fundamental frequency. Second method is a Kalman filter based approach, in which the frequency domain components of the voltage waveform are obtained by Kalman filtering. Then these components are used to obtain the light flicker. Since the frequency decomposition is obtained by Kalman filtering, no leakage effect of the DFT is involved in case of frequency deviations which is an important advantage. Both methods are tested on both simulated data and field data obtained from three different EAF plants where the flicker level and frequency variation is considerably high. The comparison with the digital realization of the IEC flickermeter shows that the methods are successful in estimating light flicker with low computational complexity. The methods are especially useful for conditions such as disturbances and subsequent system transients where the system frequency deviates significantly, since the methods avoid the need for online sampling rate adjustment to prevent the DFT leakage effect.

Keywords: flicker, electrical arc furnace (EAF), power quality (PQ), Kalman filter (KF), DFT leakage

ÖZ

ÖZGÜN SİNYAL İŞLEME ALGORİTMALARI KULLANARAK ELEKTRİK ARK OCAKLARINDA IŞIK KIRPIŞMASININ DEĞERLENDİRİLMESİ

Köse, Neslihan
Yüksek Lisans, Elektrik ve Elektronik Mühendisliği Bölümü
Tez Yöneticisi : Prof. Dr. Kemal Leblebicioğlu
Ortak Tez Yöneticisi : Dr. Özgül Salor

Eylül 2009, 81 sayfa

Bu araştırma çalışmasında, sistem frekansının saptığı durumlarda elektrik ark ocaklarında (EAO) kırpışma değerini hesaplamaya yönelik iki yeni kırpışma ölçer önerilmiştir. Bu yöntemlerde, gerilim dalgasını anlık ışık kırpışma algısına bağlayan analitik ifadelere dayanarak, IEC kırpışma ölçer standardına uygun bir kırpışma kestirim yöntemi uygulanmıştır. İlk yöntem, spektral ayrıştırma yöntemine dayalı ve Ayrık Fourier Dönüşümünün (DFT) kullanıldığı bir kırpışma hesaplama yaklaşımıdır. Bu yöntemde, temel frekanstaki değişim sebebiyle DFT algoritmasında oluşan kaçak etki, temel frekans etrafında spektral genlik düzeltme yöntemi uygulayarak azaltılmaktadır. İkincisi ise, Kalman süzgeci kullanımına dayalı bir ışık kırpışması hesaplama yöntemidir. Bu yöntemde, Kalman süzgeci kullanarak dalganın frekans spektrumundaki bileşenleri elde edilmekte ve bu bileşenler ışık kırpışmasının hesaplanması için kullanılmaktadır. Frekans ayrışımı Kalman süzgeçleme ile elde edildiğinden, frekans sapması olduğunda DFT'de oluşan kaçak etki gözlenmemektedir; bu da yöntemin sunduğu önemli bir avantajdır. Her iki yöntem de, hem sentetik veriler, hem de kırpışma dere-

cesinin ve frekans değişiminin oldukça yüksek olduğu üç farklı EAO fabrikasından toplanan saha verileri üzerinde test edilmiştir. IEC kırpışma ölçerin sayısal uyarlamasıyla yapılan karşılaştırmalar, yöntemlerin düşük hesaplama yükü ile ışık kırpışması tespitinde başarılı sonuçlar verdiğini göstermektedir. Yöntemler, özellikle sistem frekansının kaydığı bozucu etkenlerin varlığında ve bunu izleyen sistem geçici rejimleri gibi durumlar için uygundur, çünkü DFT'nin kaçak etkisini önlemek için uygulanan çevrimiçi örnekleme frekansı ayarı gereksinimi ortadan kaldırmaktadırlar.

Anahtar Kelimeler: kırpışma, elektrik ark ocağı (EAO), güç kalitesi (GK), Kalman Süzgeci (KS), DFT kaçak etkisi

To My Family

ACKNOWLEDGMENTS

I would like to express my deepest gratitude to my supervisor, Prof. Dr. Kemal Leblebicioğlu, for his guidance, advices, boundless knowledge transfer and criticism throughout this research work. I would like to thank my supervisor especially for his valuable contributions to my career.

I also would like to thank my co-supervisor, Dr. Özgül Salor, not only for her contributions and suggestions throughout this research, but also for her continuous confidence in me. Her encouragement and continuous support throughout this research work are the main reasons for the success of the study. I express my sincerest thanks to her for her guidance, companionship, support and valuable contributions during my graduate studies.

I wish to express my special thanks to Prof. Dr. Muammer Ermiş for his guidance, encouragement and valuable contributions to my career.

I would like to thank Prof. Dr. Işık Çadırcı for her support, comments and suggestions during my graduate studies.

This research work is carried out through the National Power Quality Project of Turkey in TÜBİTAK-UZAY Power Electronics Group. I would like to thank the Public Research Institutions and Development Projects Support Group (KAMAG) of the TÜBİTAK for full financial support of the project.

Special thanks to mobile power quality measurement team of National Power Quality Project of Turkey for obtaining the field data which I have used in the research work.

I would like to acknowledge my friends in Power Electronics Group of TÜBİTAK UZAY for their companionship and also for the sincere job environment provided by them.

I also would like to thank all other my friends who have been with me during this period. Their friendship, their encouragement and their trust in me are always very important for me.

Finally, I would like to thank my dearest family, my father Şükrü, my mother Birsen and my sister Burcu for their continuous support, but especially for their trust in me that I could accomplish this task during this period. I always feel lucky to have such a lovely family, I love you all...

TABLE OF CONTENTS

LIST OF TABLES

TABLES

LIST OF FIGURES

FIGURES

CHAPTER 1

INTRODUCTION

1.1 General

Light flicker resulting from frequently recurring, low amplitude voltage fluctuations is one of the major power quality disturbances in a power system. Light flicker is due to the fluctuation of the voltage amplitude supplying the incandescent lamps inside such a frequency and amplitude range that it causes annoying effect on human-beings. Such a fluctuation is usually caused by variable loads in the medium or high (MV or HV) voltage side such as arc furnaces and ladle furnaces, or by variable loads on the LV side such as X-ray equipment or copying machines. Therefore, it is a fact that voltage fluctuations caused by rapidly changing loads in the power system may cause noticeable light flicker. Up to now, researches have shown that human eye is sensitive to voltage fluctuations below $50Hz$. Especially voltage fluctuations between $0.5Hz$ and $25Hz$ cause annoying effect on human beings.

IEC (International Electrotechnical Commission) has standardized the light flicker measurement, which employs weighting curves that simulate the human eye-brain response to light fluctuations caused by an incandescent lamp [1]. The IEC standard assumes a continuous voltage input and outputs a continuous instantaneous flicker sensation, and a discrete output, which is called the short term flicker severity. On the other hand, several approaches have been used to estimate the instantaneous flicker sensation and the flicker severity when the input is a sampled form of the continuous voltage [2]-[9]. Most of these approaches use the frequency domain decomposition of the voltage waveform to obtain the instantaneous flicker sensation [2]-[6]. The problem with frequency domain approaches is that they usually employ DFT to obtain the frequency decomposition, which suffers from picket-fence effect and leakage due to the fundamental frequency deviations and the windowing effect in the digital domain [4]. To solve this problem, various approaches have been proposed including indirect demodulation method [6], smart DFT [2] and wavelet transforms [3]. In indirect demodulation method, initially the envelope of the voltage waveform is obtained and then DFT algorithm is applied on this envelope. Therefore, no leakage effect problem due to fundamental frequency deviation occurs [6]. Smart DFT is also another approach to solve the leakage problems. Smart DFT smartly avoids the errors that arise when fundamental frequency deviates and keeps the advantages of the DFT algorithm [2]. In [3], a wavelet transform approach is proposed to estimate the light flicker, which is considerably robust to fundamental frequency deviations. These approaches are usually compared to the digital realizations of the IEC flickermeter [9] and quite satisfactory results are obtained at the expense of computational complexity.

1.2 Problem Definition and Scope of the Thesis

Up to now, researches have shown that the system frequency deviates significantly due to the EAF operation. Power quality measurements realized nationwide have shown that the $50Hz$ system frequency deviates within a band of $50\pm0.2Hz$ at the MV side of the busbar supplying the EAFs [10]. It has been reported in the literature that the actual system frequency may deviate from the normal value due to various reasons such as disturbances, subsequent transients and or the dramatic real power fluctuations of arc furnace plants [3, 11, 12, 13, 14]. In [3], it is reported that field tests performed in a steel plant in southern Taiwan, it was observed that the frequency of R-phase voltage measurement changes from $59.92Hz$ to $60.12Hz$, where the nominal frequency is $60.0Hz$. In [11], it is reported that the most preferable frequency deviation is $\pm0.02Hz$; however, for case studies such as a large steel mill and an arc furnace factory, the maximum allowable change in the transient frequency lies between $\pm 0.50 Hz$. In [15], it is reported that US-wide power system frequency usually varies between $59.99Hz$ and $60.02Hz$;, however, in case of an event the frequency may drop down to $59.55Hz$. It is observed that during safe operation, the power system frequency deviates due to various reasons; but, in interconnected systems such as the US-power network [15], this deviation is much less than that of the power systems without such an interconnection [10, 11]. If a DFT-based algorithm is employed to obtain spectral decomposition of a waveform in a deviated frequency case, leakage effect occurs and to overcome the leakage effect, generally two methods can be used. The first one is to adjust the sampling frequency such that the same number of samples cover the same number of frequency cycles. This can be achieved, for example, using a phase-locked-loop controlling the sampling process. The second one is to use a fixed-length window with different spectral techniques to obtain a better frequency spectrum estimate [2, 3, 6]. In this research work, two new methods are proposed to estimate spectral components of voltage waveforms and consequently the light flicker where the system frequency deviates significantly due to the EAF operation. In the proposed methods, after obtaining the spectral components, the light flicker caused by electric arc furnace (EAF) plants at the MV side is calculated by using these spectral components.

Harmonics and interharmonics are frequently observed in power systems. Harmonic frequency is the frequency which is an integer multiple of the fundamental frequency ($50Hz$ or $60Hz$), whereas interharmonic frequency is the frequency which is not an integer multiple of the fundamental frequency [16]. Several interharmonics and harmonics are observed on the data collected from EAF plants. Spectral analysis of harmonics and interharmonics of the power signals are usually done by using the Fast Fourier Transform (FFT) algorithm due to its computational complexity. Figure 1.1 shows the harmonics (up to 5. harmonic, which is $250Hz$ for $50Hz$ power system) and interharmonics of a $200ms$-length field data which are obtained by applying FFT algorithm on the voltage data of an EAF plant. Interharmonics are the real cause of light flicker in power systems. Flicker-causing interharmonics can be observed clearly in the frequency spectrum of the specified voltage waveform as shown in Figure 1.1.

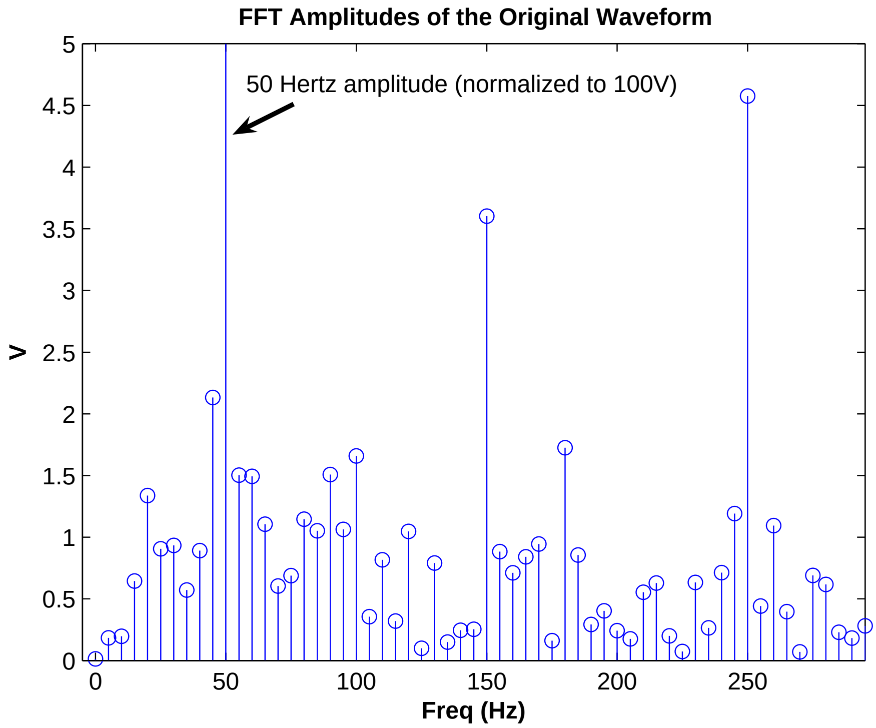

Figure 1.1: An example showing harmonics and interharmonics of an AC arc furnace data.

In this research work, both of the proposed methods are spectral decomposition based methods to obtain flicker-causing interharmonics. The models proposed in both of these methods are based on the IEC flickermeter explained in the IEC Standard 61000-4-15 [1], whose block diagram is given in Figure 2.1. Both proposed methods simulate the IEC flickermeter computation beginning from the normalized voltage input (input to Block - 2 in Figure 2.1) to Output-5 which outputs S in digital domain. In these methods, a frequency domain approach is proposed to estimate the light flicker. The main difference between the two proposed methods is that; to obtain the frequency spectrum of the voltage waveform, considerably different approaches are applied. In the first method, spectral decomposition is obtained by utilizing the DFT algorithm on the voltage waveform using $200ms$ time windows (10 cycles for a $50Hz$ system), which coincides with the IEC harmonic and interharmonic computation standard [16]. However due to the system frequency deviation, leakage effect is observed when DFT algorithm is applied. The leakage effect of the DFT algorithm due to frequency variation is taken care of by employing a novel spectral amplitude correction procedure around the fundamental frequency [7, 17]. The correction procedure is based on estimating the system frequency at consecutive windows and synthesizing a pure sinusoidal signal with the same frequency so as to obtain the leakage effect caused by the system frequency deviation. The leakage is then vector-subtracted for each interharmonic around the fundamental frequency and corrected frequency spectrum is obtained. In the second method, on the other hand, spectral decomposition is obtained by applying two Kalman filters consecutively in succession on the voltage waveform again using $200ms$ time windows as recommended in the IEC harmonic and interharmonic computation standard [16]. Initially, an EKF is used to obtain the voltage envelope and then a second Kalman filter, which is a LKF this time, is used to obtain the spectral components around the fundamental out of the envelope of the voltage waveform causing flicker [18]. After the spectral components are obtained by the Kalman filters, the light flicker is evaluated using these components as proposed in the first method, which is also explained in [7, 19]. Since in the second method, no DFT algorithm is used, no leakage effect problem is involved in case of fundamental frequency deviations. Therefore there is no need for extra work to obtain a corrected spectrum, which is an important advantage and novelty of the second method.

In both of the proposed methods, the eye-brain weighting curve of the IEC flickermeter is realized by comparing the voltage spectrum with the tabulated normalized flickermeter responses for sinusoidal voltage fluctuations of the IEC standard [1]. Both of the proposed methods are tested on both simulated data and field data obtained from three different EAF plants. The comparison with the digital realization of the IEC flickermeter shows that the proposed methods give satisfactory estimations of both the instantaneous flicker sensation and the short term flicker severity with low computational complexity. Therefore, the proposed methods can be considered as two new flickermeter applications.

This thesis is organized as follows: Chapter 2 gives a brief overview of the IEC flicker determination approach applied to a discrete voltage waveform, on which the proposed methods are based. The first proposed method, a new spectral decomposition based approach for flicker evaluation of electric arc furnaces, with algorithm improvements are also described in this chapter. In Chapter 3, the second proposed method, a Kalman Filtering Based Approach for Light Flicker Evaluation of Power Systems is presented. The comparison between the two proposed methods on AC arc furnace data is also given in this chapter. Finally in Chapter 4, conclusions and future directions are provided.

CHAPTER 2

A NEW SPECTRAL DECOMPOSITION BASED APPROACH FOR FLICKER EVALUATION OF ELECTRIC ARC FURNACES

The proposed spectral decomposition based approach, which is also explained in [7], is attributed to the mathematical relationship derived between the input waveform of the IEC flickermeter and the measured instantaneous flicker sensation. Therefore, this chapter briefly explains the IEC flickermeter design first, then it presents the mathematical derivations followed by the proposed method.

2.1 The IEC Flickermeter

Both of the methods proposed in this thesis are based on the IEC flickermeter explained in the IEC Standard 61000-4-15 [1]. The IEC flickermeter block diagram is given in Figure 2.1. The major parts of the IEC flickermeter are the input processing part, the lamp-eye-brain response part, and the output processing part. There are two primary steps in input processing part. First step is for converting the rms value of measured voltage to a reference level in order to guarantee that percentage deviations are equal regardless of the input rms level. In second step, the square of the input is obtained by the square demodulator to separate the low frequency ($0.5-25Hz$) components from the power frequency components through filtering. Then comes the lamp-eye-brain response part. In this part, the lamp-eye-brain characteristic is obtained from mathematical derivation of the response of a lamp to a supply voltage variation,

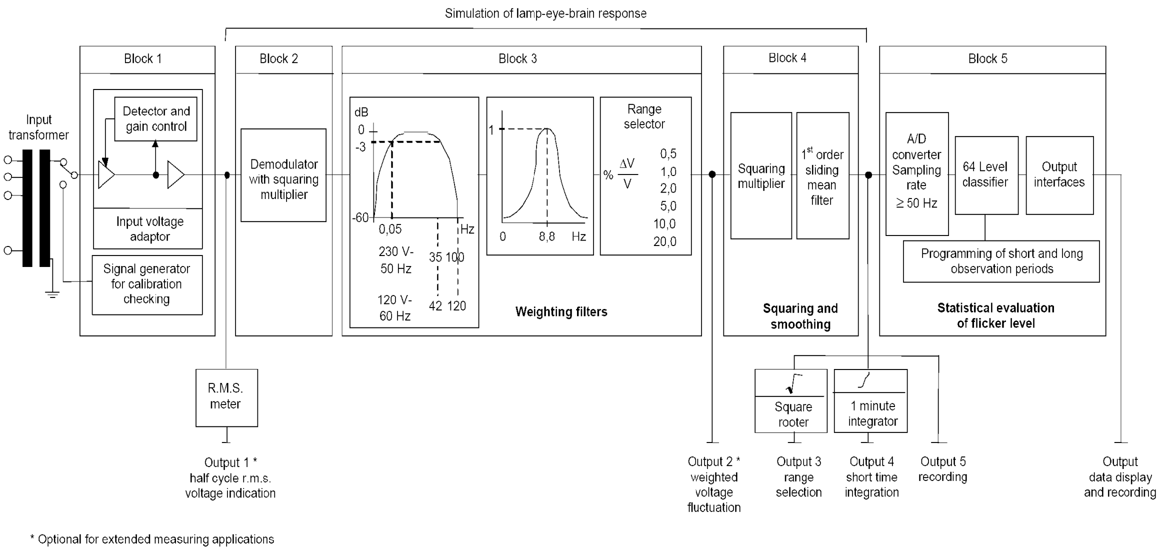

Figure 2.1: Block diagram of the IEC flickermeter.

the perception ability of the human eye and the memory tendency of a human brain. Finally in output processing part, the output of Block 4, instantaneous flicker sensation is translated into the statistical index, P_{st}. Therefore, the IEC flickermeter can be basically explained as; the IEC procedure for light flicker computation initially scales the input voltage down to the last minute rms value before it simulates the response of the lamp-eye-brain chain by a square law demodulator followed by weighting filters and a range selector. Then follows the squaring multiplier and the sliding mean filter blocks, which simulate the non-linear eye-brain perception and the storage effect of the human brain, respectively. The result gives the instantaneous flicker sensation, denoted by S, which is a continuous waveform (Output - 5 in Figure 2.1). Then S is sampled and put into a statistical evaluation block to obtain the short term flicker severity, P_{st}, which is computed for non-overlapping data windows of 1, 2, 10 or 15 minutes. The short term flicker severity index, P_{st}, is a statistical quantification of the instantaneous flicker sensation, S. The proposed methods in this thesis simulate the IEC flickermeter computation beginning from the normalized voltage input (input to Block - 2 in Figure 2.1) to Output-5 which outputs S in digital domain.

2.2 Derivation of the Mathematical Relationship between the Input Voltage and the Flicker Sensation

The model proposed in this approach is based on the IEC flicker evaluation standard [1], whose block diagram is given in Figure 2.1. The IEC standard [1] considers the flicker-causing fluctuation of the voltage as an AM modulated signal, where the power system frequency (50 or $60Hz$) is the carrier frequency and the flicker frequency is the message frequency as given in

$$v(t) = V sin(2\pi ft)\left\{1 + \frac{1}{2}\frac{\Delta V}{V} sin(2\pi f_f t + \phi)\right\} \tag{2.1}$$

where f is the power system (fundamental) frequency, $\Delta V/V$ is the relative voltage fluctuation, f_f is the flicker frequency, and ϕ is the phase. An example waveform showing the flicker-causing fluctuation of the voltage with $V = 1$, $\frac{\Delta V}{V} = 0.2$, $f = 50Hz$, and $f_f = 5Hz$, is given in Figure 2.2. For the general case of a more complicated voltage fluctuation as observed in the supply voltages of the EAF plants, the input voltage to the flickermeter can be expressed as

$$v(t) = V sin(2\pi ft)\left\{1 + \sum_{i=1}^{N}\frac{\Delta V_i}{2V} sin(2\pi f_{fi} t + \phi_i)\right\} \tag{2.2}$$

where N is the number of flicker frequencies, f_{fi} are flicker frequencies, and ϕ_i are the corresponding phases. The effect of the modulation appear as interharmonics

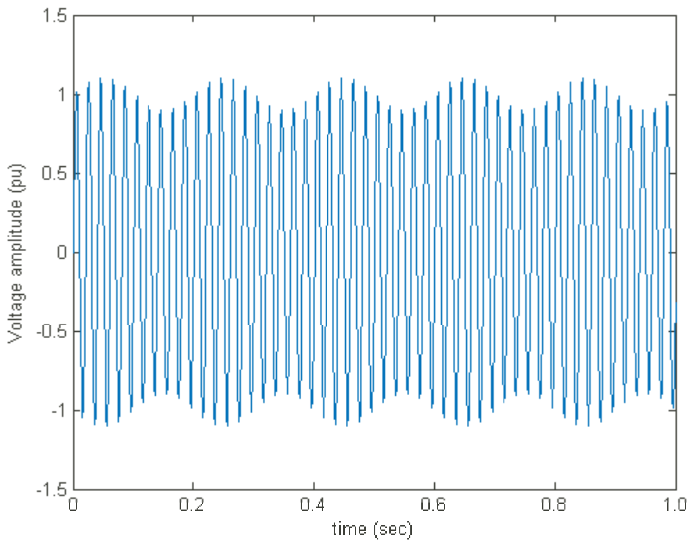

Figure 2.2: An example waveform showing the flicker-causing fluctuation of the voltage

at beat frequencies which are $f \mp f_{fi}$ in the spectrum since (2.2) can be rewritten as given in

$$v(t) = Vsin(2\pi ft) + \sum_{i=1}^{N} \frac{\Delta V_i}{4} \left\{cos(2\pi(f - f_{fi})t + \phi_i) - cos(2\pi(f + f_{fi})t + \phi_i)\right\}. \tag{2.3}$$

It is observed from (2.3) that the frequency spectrum of the voltage waveform can be used to obtain the flicker causing interharmonic frequencies and their magnitudes. In the following paragraphs, instantaneous flicker sensation computation method of the IEC flickermeter will be applied to (2.2), to obtain the relationship between the flicker frequencies and the instantaneous flicker sensation, S.

2.2.1 Square Demodulation and Lamp-Eye-Brain Filters

The square demodulation is applied to the signal given in (2.2) assuming the $v(t)$ is the normalized input waveform (input to the Block-2 in Figure 2.1)

$$v^2(t) = V^2 sin^2(2\pi ft) \left(1 + \sum_{i=1}^{N} \frac{\Delta V_i}{2V} sin(2\pi f_{fi} t + \phi_i)\right)^2 \tag{2.4}$$

which can be rewritten as

$$\begin{aligned} v^2(t) \quad = \quad & \frac{1}{2}V^2(1 - cos(2\pi 2ft)) \left\{1 + \sum_{i=1}^{N} \left(\frac{\Delta V_i}{2V}\right)^2 sin^2(2\pi f_{fi} t + \phi_i)\right. \\ & +2\sum_{i=1}^{N} \sum_{j=i+1}^{N} \frac{(\Delta V_i)(\Delta V_j)}{4V^2} sin(2\pi f_{fi} t + \phi_i) sin(2\pi f_{fj} t + \phi_j) \\ & \left. +2\sum_{i=1}^{N} \frac{\Delta V_i}{2V} sin(2\pi f_{fi} t + \phi_i)\right\}. \end{aligned} \tag{2.5}$$

The lamp-eye-brain chain filters are cascaded to filter the waveform given in (2.5), whose overall response conform with band-pass filter characteristics achieving its peak magnitude at $8.8Hz$. The frequencies larger than $35Hz$ and the dc terms are filtered out completely [1]. Therefore, the high frequency components which appear with the modulating effect of the $cos(2\pi 2ft)$ ($f = 50$ or $60Hz$) term in (2.5) will fade away at the output in addition to the dc terms. The filtered form of (2.5) can be approximated as

$$
\begin{aligned}
v_F^2(t) \quad = \quad & -\frac{V^2}{2}\sum_{i=1}^{N}\frac{(\Delta V_i)^2}{2(2V)^2}H(2f_{fi})cos(2\pi 2f_{fi}t+2\phi_i) \\
& +\frac{V^2}{2}\sum_{i=1}^{n}\sum_{j=i+1}^{n}\frac{(\Delta V_i)(\Delta V_j)}{4V^2}\left[H(f_{fi}-f_{fj})cos(2\pi(f_{fi}-f_{fj})t+\phi_i-\phi_j)-H(f_{fi}+f_{fj})cos(2\pi(f_{fi}+f_{fj})t+\phi_i+\phi_j)\right] \\
& +\frac{V^2}{2}\sum_{i=1}^{N}\frac{\Delta V_i}{V}H(f_{fi})sin(2\pi f_{fi}t+\phi_i). \qquad (2.6)
\end{aligned}
$$

where $H(f_{fi})$ is the combined frequency response of the lamp-eye-brain filters at frequency f_{fi}.

In (2.6), the terms with $\frac{(\Delta V_i)^2}{8V^2}$ and $\frac{(\Delta V_i)(\Delta V_j)}{4V^2}$ multipliers will be negligible when compared to the term which has the multiplication factor $\frac{\Delta V_i}{V}$, since $\frac{\Delta V_i}{V}$ value does not usually exceed 0.1 in any arc furnace voltage measured to date. Even in the worst case of $\frac{\Delta V_i}{V}=0.5$, $\left(\frac{(\Delta V_i)^2}{4V^2}\right)/\left(\frac{\Delta V_i}{V}\right)=1/8$. Therefore, the first and the second terms are neglected in (2.6), before proceeding to the squaring multiplier and the first order sliding mean filter. The squaring in the next step will also emphasize the last term of (2.6). Therefore (2.6) is approximated as

$$
v_F^2(t) \quad \approx \quad \sum_{i=1}^{N}\frac{V(\Delta V_i)H(f_{fi})}{2}sin(2\pi f_{fi}t+\phi_i). \qquad (2.7)
$$

2.2.2 Squaring Multiplier and Sliding Mean Filter

The squaring multiplier output is the squared form of (2.7) which is expressed as

$$
\begin{aligned}
v_F^4(t) \quad = \quad & \frac{V^2}{8}\sum_{i=1}^{N}(\Delta V_i)^2H^2(f_{fi})-\frac{V^2}{8}\sum_{i=1}^{N}(\Delta V_i)^2H^2(f_{fi})cos(2\pi 2f_{fi}t+2\phi_i) \\
& +\frac{V^2}{4}\sum_{i=1}^{N}\sum_{j=i+1}^{N}((\Delta V_i)H(f_{fi}))((\Delta V_j)H(f_{fj}))cos(2\pi(f_{fi}-f_{fj})+\phi_i-\phi_j) \\
& -\frac{V^2}{4}\sum_{i=1}^{N}\sum_{j=i+1}^{N}((\Delta V_i)H(f_{fi}))((\Delta V_j)H(f_{fj}))cos(2\pi(f_{fi}+f_{fj})+\phi_i+\phi_j). \qquad (2.8)
\end{aligned}
$$

In (2.8), it is observed that at the output of the squaring multiplier of the IEC flickermeter, there are dc components, components at twice the flicker frequencies and components at summations and differences of all possible flicker frequency pairs. The sliding mean filter following the squaring multiplier is a first order low pass filter with time constant $\tau = 300ms$ [1]. This filter, whose output is the instantaneous flicker sensation, can be approximated as follows [20]:

$$S = \frac{1}{\tau}\int^{\tau} v_F^4(t)\cdot dt. \tag{2.9}$$

Therefore, instantaneous flicker sensation, S, will be dominated by the dc term in (2.8) which is $(\frac{V^2}{8}\sum_{i=1}^{N}(\Delta V_i)^2 H^2(f_{fi}))$ with ripples fluctuating every $300ms$ and hence instantaneous flicker sensation, S, can be approximated as

$$S \approx \frac{V^2}{8}\sum_{i=1}^{N}(\Delta V_i)^2 H^2(f_{fi}). \tag{2.10}$$

From (2.10) it is observed that the effect of individual flicker frequencies on the instantaneous flicker sensation is approximately additive. Also phase differences between different flicker frequencies have negligible effect on S. This fact has also been pointed out based on experimental measurements by Keppler, et.al. [21].

2.2.3 Instantaneous Flicker Sensation Determination and the Proposed Method

The IEC flickermeter response for sinusoidal fluctuations (frequencies and $\Delta V/V$ ratios) which result in unity instantaneous flicker sensation ($S = 1$) are given for both $230V/50Hz$ and $120V/60Hz$ systems in [1]. The proposed light flicker estimation method is applicable to both types of systems. In this research work, $230V/50Hz$ system is considered for field measurements since the field data obtained are collected at EAF plants operating at $50Hz$ systems. Table 2.1 provides the flickermeter response of IEC for sinusoidal voltage fluctuations in a $230V/50Hz$ power system.

S is approximately the summation of the flicker-causing effects of the individual flicker frequencies as given in (2.10). Contribution of each flicker frequency to S, which is represented here by S_i, can be determined by comparing the square of the $\Delta V/V$ values obtained from the FFT of the voltage waveform in (2.3) to the square of the $\Delta V/V$ values obtained from Table 2.1 as

$$S_i = \frac{\frac{V^4}{8}\left(\frac{\Delta V_i}{V}\right)^2 H^2(f_{fi})}{\frac{V^4}{8}\left(\frac{\Delta V_i}{V}\right)^2_{IEC} H^2(f_{fi})} = \frac{\left(\frac{\Delta V_i}{V}\right)^2}{\left(\frac{\Delta V_i}{V}\right)^2_{IEC}} \tag{2.11}$$

where $\left(\frac{\Delta V_i}{V}\right)_{IEC}$ is obtained from Table 2.1 for the flicker frequency f_{fi} and $\frac{\Delta V_i}{V}$ is obtained from the amplitudes of the FFT of the voltage waveform given in (2.3). Frequencies around the fundamental frequency are considered ($f - 25Hz$ to $f + 25Hz$), where $25Hz$ is the maximum flicker frequency given in Table 2.1. Contributions of frequencies below $f - 25Hz$ and above $f + 25Hz$ are negligible. Then S is obtained as the summation of all S_i, $S = \sum_{i=1}^{N} S_i$, where f_{fi} varies from $0.5Hz$ to $25.0Hz$ with $0.5Hz$ increments when the FFT window size is 100 cycles long. However, a duration of 100 cycles is too long when the non-stationary behavior of the EAF operation is considered. The IEC Standard for harmonics and interharmonics computation requires the FFT window sizes to be 10 cycles long [16]. Therefore, the algorithm is tested with both 100-cycle and 10-cycle long FFT-windows on simulated data and with 10-cycle long windows

Table 2.1: Normalized Flickermeter Response for Sinusoidal Voltage Fluctuations, 230V/50Hz system - IEC Standard 61000-4-15

Hz	$\Delta V/V$ (%)	Hz	$\Delta V/V$ (%)
0.5	2.340	10.0	0.260
1.0	1.432	10.5	0.270
1.5	1.080	11.0	0.282
2.0	0.882	11.5	0.296
2.5	0.754	12.0	0.312
3.0	0.654	13.0	0.348
3.5	0.568	14.0	0.388
4.0	0.500	15.0	0.432
4.5	0.446	16.0	0.480
5.0	0.398	17.0	0.530
5.5	0.360	18.0	0.584
6.0	0.328	19.0	0.640
6.5	0.300	20.0	0.700
7.0	0.280	21.0	0.760
7.5	0.266	22.0	0.824
8.0	0.256	23.0	0.890
8.8	0.250	24.0	0.962
9.5	0.254	25.0	1.042

on field data. In case of 10-cycle windows, f_{fi} varies from $5Hz$ to $25Hz$ with $5Hz$ increments.

S obtained from S_i for $200ms$ windows overlapping $180ms$ or 9 cycles, which means sampling frequency of S is $50Hz$, represent the stationary behaviour of the sliding mean filter given in (2.9). When a higher sampling rate of S is required, the sliding mean filter can be approximated by filtering S with the sliding mean filter as proposed by [5]. In this method, a sampling rate of $50Hz$ is used for S as recommended smallest rate in [1] to reduce the computational complexity.

2.3 Correction of the Spectral Components for Deviated Frequency Case

DFT is a powerful and efficient algorithm to obtain the frequency distribution of the voltage waveform. However, DFT suffers from leakage effect [3, 4], when there exist fundamental frequency deviation. In this part, initially formulation of the leakage effect of the DFT is given, after that the proposed approach for correction of the spectral components is explained.

2.3.1 Formulation of Leakage Effect of the Discrete Fourier Transform

To formulate the spectral leakage problem of the DFT, the continuous time signal with a single frequency component is considered:

$$v(t) = V_f cos(\omega_f t), \tag{2.12}$$

where ω_f is the fundamental frequency of the power signal ($\omega_f = 2\pi f_f$) and V_f is the corresponding amplitude. Cosine is preferred here instead of sine to make the Fourier transform equations simpler, and this does not cause any loss of generality. Since the signals are analyzed in digital domain, this signal is sampled with a sampling frequency f_s, which is higher than the Nyquist frequency, and a finite number of samples N is used for the Fourier analysis. This corresponds to windowing the signal in (2.12) with a rectangular window of duration $T = N/f_s$. The windowed form of the signal is shown as:

$$v_w(t) = V_f cos(\omega_f t) \cdot w(t), \tag{2.13}$$

where $w(t)$ is the window function, which equals to unity for $0 < t < T$, and equals to zero elsewhere. The Fourier transform of the rectangular window function is:

$$W(\omega) = \frac{sin(\omega T/2)}{\omega/2} e^{-j\omega T/2}, \tag{2.14}$$

while the Fourier transform of $v(t)$ equals

$$V(\omega) = \pi V_f [\delta(\omega - \omega_f) + \delta(\omega + \omega_f)]. \tag{2.15}$$

Since the windowed function is obtained by multiplying the signal $v(t)$ with the window function $w(t)$, the Fourier transform of the windowed function is obtained by convolving their Fourier transforms as:

$$V_w(\omega) = \pi V_f \int W(\omega - \tau)[\delta(\tau - \omega_f) + \delta(\tau + \omega_f)] d\tau. \tag{2.16}$$

For a rectangular window, the peak appears at ω_f and the zero crossing points are at $\omega = \omega_f + k2\pi/T$. If the signal is sampled at $f_s = N/T$, the samples in frequency domain correspond exactly to the points at frequencies $\omega = \omega_f + k2\pi/T$ according to (2.14) and only the component at ω_f is non-zero in the sampled spectrum, which is the DFT of the sampled form of $v_w(t)$, and hence there is no leakage effect caused by rectangular windowing. On the other hand, if the sampling frequency slightly differs from N/T, leakage components appear in the spectrum due to windowing at frequencies around $\omega = \omega_f + k2\pi/T$ and these components are not zero, indicating that interharmonics exist but in fact the signal $v(t)$ has no interharmonic components.

If the signal $v(t)$ contains interharmonics as given in

$$v(t) = V_f cos(\omega_f t) + V_1 cos[(\omega_f + \triangle\omega_1)t + \phi_1] + V_2 cos[(\omega_f + \triangle\omega_2)t + \phi_2], \tag{2.17}$$

where V_1 and V_2 are the interharmonic amplitudes, $\omega_f + \triangle\omega_1$ and $\omega_f + \triangle\omega_2$ are the interharmonic frequencies and ϕ_1 and ϕ_2 are the corresponding phases, then the Fourier transform of (2.17) becomes

$$\begin{aligned} V(\omega) = \;& \pi V_f[\delta(\omega-\omega_f)+\delta(\omega+\omega_f)] \\ & +\pi V_1[\delta(\omega-\omega_f-\triangle\omega_1)+\delta(\omega+\omega_f+\triangle\omega_1)] \\ & +\pi V_2[\delta(\omega-\omega_f-\triangle\omega_2)+\delta(\omega+\omega_f+\triangle\omega_2)]. \end{aligned} \tag{2.18}$$

The Fourier transform of the windowed signal can be obtained as:

$$\begin{aligned} V_w(\omega) = \;& \pi V_f \textstyle\int W(\omega-\tau)[\delta(\tau-\omega_f)+\delta(\tau+\omega_f)]d\tau \\ & +\pi V_1 \textstyle\int W(\omega-\tau)[\delta(\tau-\omega_f-\triangle\omega_1)+\delta(\tau+\omega_f+\triangle\omega_1)]d\tau \\ & +\pi V_2 \textstyle\int W(\omega-\tau)[\delta(\tau-\omega_f-\triangle\omega_2)+\delta(\tau+\omega_f+\triangle\omega_2)]d\tau \end{aligned} \tag{2.19}$$

The first term in (2.19) is due to the fundamental component and if the sampling frequency equals to exactly N/T, this term will yield zero for frequency samples other than ω_f. On the other hand, if the fundamental frequency deviates slightly from $2\pi/T$, the first term will add leakage components to the spectrum in addition to the interharmonic terms (2^{nd} and 3^{rd} terms) given in (2.19). As observed, the leakage terms for rectangular windowing are additive and the proposed spectral correction method is based on this fact. If the fundamental frequency can be detected precisely, the leakage effect can be computed on synthetic data and then it can be subtracted from the original signal spectrum to correct the interharmonic values.

2.3.2 Correction of the Spectral Components

In the proposed algorithm, $\Delta V_i/V$ values corresponding to the flicker frequencies are obtained from the DFT of the voltage signal given in (2.3). However, DFT suffers from picket-fence effect and leakage [3, 4], when there exist interharmonic frequencies and fundamental frequency deviation. These are commonly observed in EAF plants due to the nature of the EAF operation. Observations on the field data obtained from various EAF plants [10, 22] have shown that the fundamental system frequency tends to be lower or higher than the nominal value during boring and melting phases and usually higher during the refining phases. From measurements on the field data obtained from three different EAF plants, it is observed that in EAF plants, the fundamental frequency fluctuates between

$49.7Hz$ and $50.3Hz$. In the proposed method, for the DFT computation on field data, window size is selected as $200ms$ that corresponds to the 10 cycles of the $50Hz$ fundamental frequency, which is compatible with the IEC Standard [16]. When the frequency deviates from the nominal value, the window size is not an integer multiple of the actual cycle any more and this causes leakage effect on the DFT components.

To observe the leakage effect, the algorithm is tested with simulated voltage waveform, with sinusoidal voltage fluctuation as given in (2.1) with flicker frequency $f_f = 10Hz$, and $\Delta V/V = 0.260\%$ as it is given in Table 2.1 and fundamental frequency f varying from $49.5Hz$ to $50.5Hz$. The whole data duration is selected to be 10 minutes and P_{st} is obtained from the resulting instantaneous flicker sensation, S. S is computed on every 10-cycle period with 9-cycle overlapping sliding windows with the proposed algorithm so that the sampling rate of S is $50Hz$ as required in the IEC Standard [1]. S is expected to fluctuate around unity; however, due to the deviation in the fundamental frequency, leakage causes incorrect predictions of S when fundamental frequency deviates from $50Hz$. The results are given in Table 2.2 under the column "*Without Spectral Correction*". S values given in Table 2.2 are the mean values of the S array obtained for 10-minute long data. It is shown that the algorithm results in $S = 1$ when the fundamental frequency is exactly $50Hz$. The leakage effect for fre-

Table 2.2: Effect of the System Frequency Deviation

$f(Hz)$	Without Spectral Correction		With Spectral Correction	
	$mean(S)$	P_{st}	$mean(S)$	P_{st}
49.5	17718.27	93.29	1.01	0.70
49.6	11256.69	74.22	1.01	0.70
49.7	6296.20	55.42	1.00	0.70
49.8	2787.41	36.82	1.00	0.70
49.9	695.88	18.37	1.00	0.69
50.0	1.00	0.69	1.00	0.69
50.1	695.84	18.31	1.00	0.69
50.2	2787.08	36.59	1.00	0.70
50.3	6295.04	54.90	1.00	0.70
50.4	11245.18	73.43	1.01	0.70
50.5	17713.65	92.24	1.01	0.70

quency deviations on S, in a smaller range from $49.9Hz$ to $50.1Hz$ with $0.01Hz$ increments, when a fixed $200ms$-length window is used, is also illustrated in Figure 2.3. S is found to be as high as 700, where it actually should have been found around unity if no leakage existed.

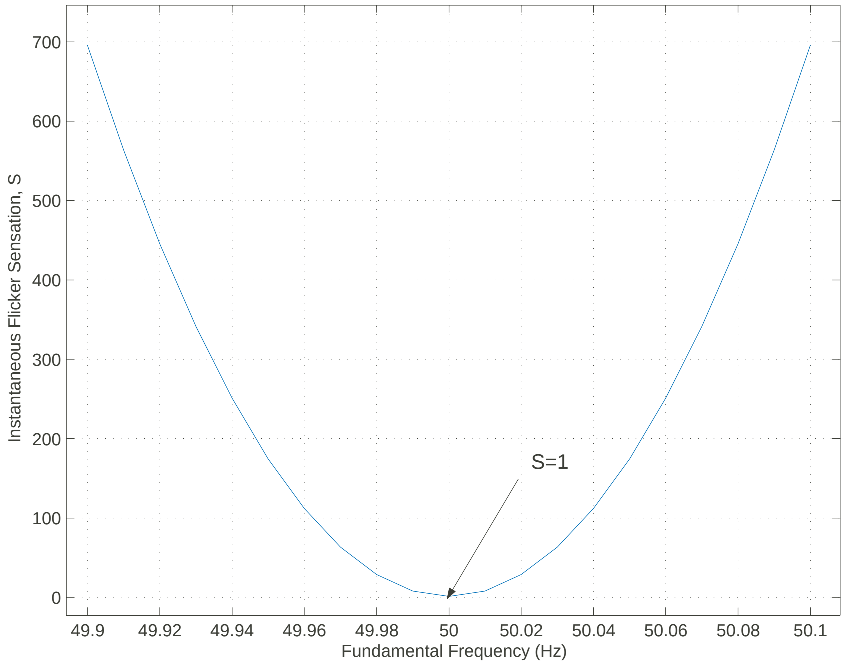

Figure 2.3: The leakage effect for frequency deviations on the instantaneous flicker sensation, S. Fundamental frequency is changed from $49.9Hz$ to $50.1Hz$ with $0.01Hz$ increments. $200ms$-length window is used for DFT computation.

The reason of the high error given in Table 2.2 is that the individual effects coming from each frequency are squared and summed up as given in (2.10). The leakage of the DFT is illustrated in Figure 2.4 for the same signal with the same flicker frequencies as given in Table 2.2. The corresponding S, whose average values are given in Table 2.2, values are given in Figure 2.5. This figure shows the quadratic increase in S as the fundamental frequency deviates from the nominal value.

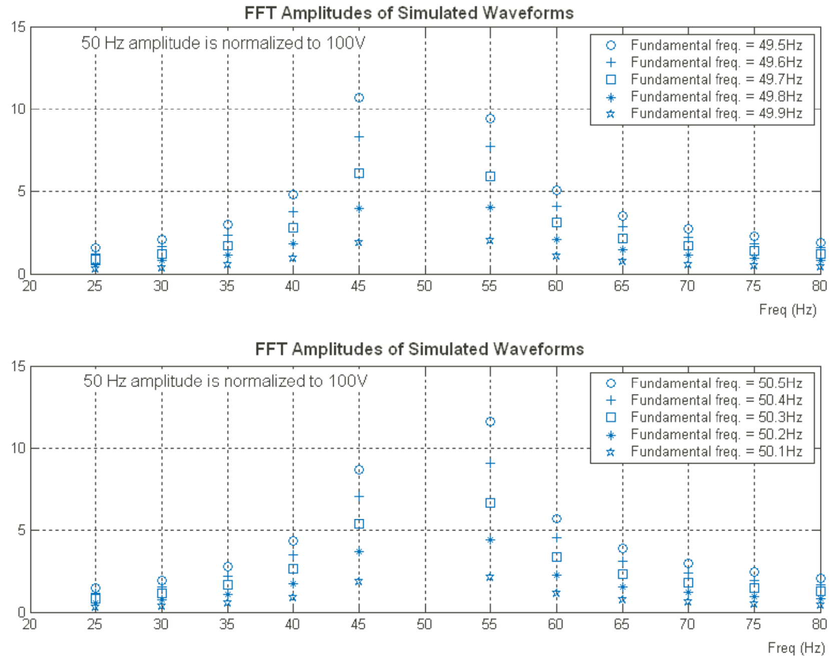

Figure 2.4: DFT leakage effect on the amplitude characteristics for the fundamental frequency values given in Table 2.2.

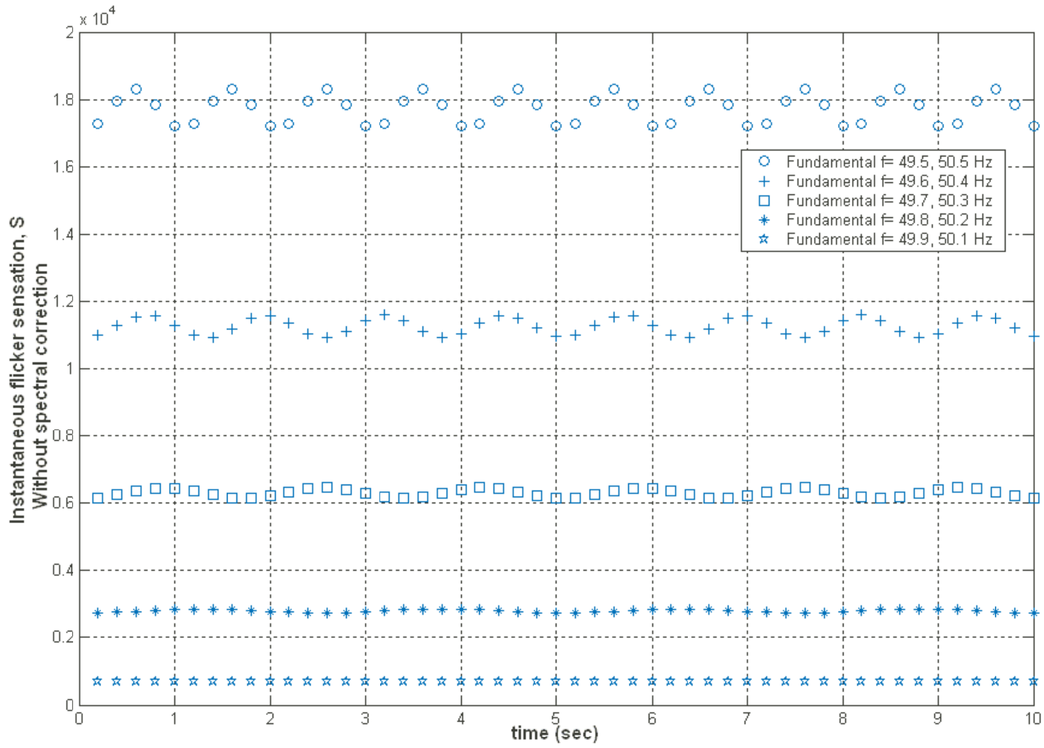

Figure 2.5: S computed out of the DFT values given in Figure 2.4 for a data of $10 sec.$ long without spectral correction.

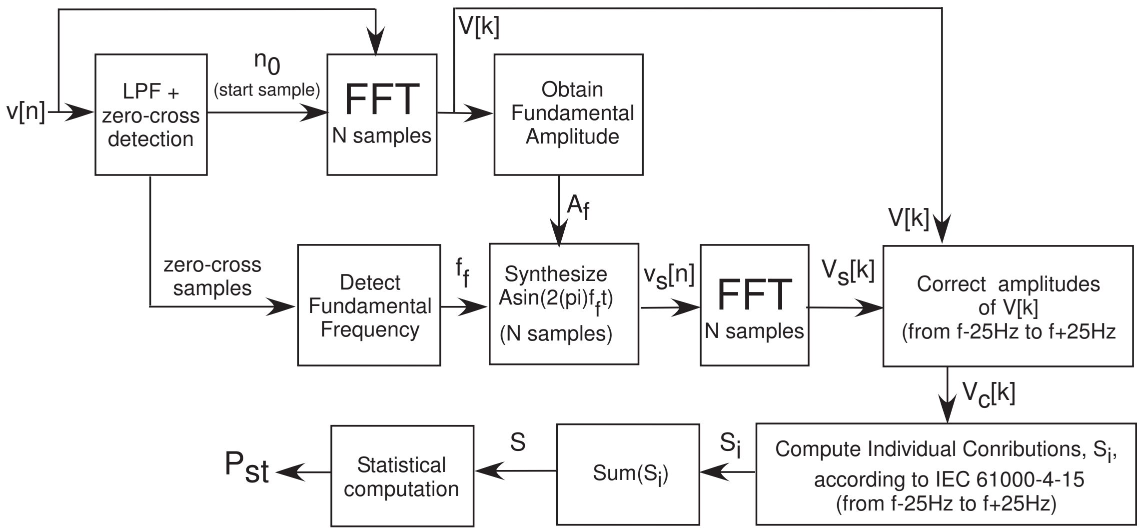

Figure 2.6: Block diagram of the proposed flicker estimation method.

The block diagram of the proposed light flicker estimation method is given in Figure 2.6. Assume that the sampled input signal is denoted by $v[n]$. Since FFT algorithm is used to realize DFT computation in this thesis, from now on FFT will be used to explain the details of the algorithm. To go to the frequency domain through FFT, a standard window length, N samples, is used assuming the fundamental frequency does not deviate from the nominal value ($200ms$ or $2s$ for 10-cycle or 100-cycle windows, respectively). The recommended window length is 10 cycles for a $50Hz$ power system in the standard IEC-61000-4-7 [16]. $N = 640$ for the sampling rate of $3200Hz$. The beginning of the window is adjusted such that it starts at the nearest zero-crossing, n_0, from negative to positive side of the signal, so that the phase of the fundamental component is zero. To obtain the zero-crossings a low pass filter (LPF) with a corner frequency at $75Hz$, which cleans the signal from the harmonic and interharmonic effects, is applied first. Then the zero-crossings are determined and FFT of the $N-sample$ signal is computed which is represented by $V[k]$ in Figure 2.6. However, this FFT contains spectral estimation errors if the fundamental frequency deviates from the nominal value.

In order to get rid of these spectral estimation errors, a good estimation of the fundamental frequency is necessary. The exact fundamental frequency is computed by applying correction to the first and the final zero-crossings as given

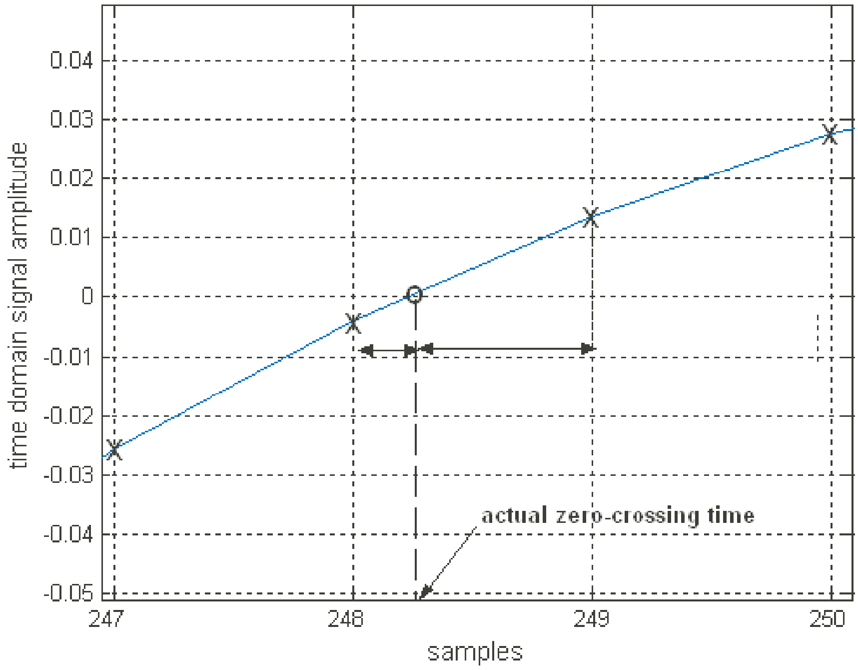

Figure 2.7: Zero-crossing correction [23].

in [24]. This correction is illustrated in Figure 2.7 on an example zero-crossing. The exact zero-crossing is determined by applying a linear interpolation between the two samples as given in Figure 2.7, where Xs show the samples of the signal and Os show the actual zero-crossing of the signal, which is computed both at the beginning and the end of the 10-cycle period for correct fundamental frequency computation. Then to obtain a better spectrum, a pure sinusoidal waveform of the same frame length, N, is synthesized with the amplitude of the fundamental A_f and the computed fundamental frequency, f_f, as $v_s[n] = A_f sin(2\pi f_f t)$. As explained in [23], the amplitude A_f is different from the amplitude measured from the DFT algorithm, if there is frequency deviation as observed in Figure 2.8. Therefore, the correct value of A_f at the exact fundamental frequency, f_f, is computed from:

$$2\pi AT = \left| \pi A_f \int W(w_n - \tau) \left[\delta\tau - w_f + \delta(\tau + w_f) \right] d\tau \right| , \tag{2.20}$$

Since the signals are analyzed in digital domain, signal is sampled with a sampling frequency f_s, which is higher than the Nyquist frequency in order to prevent the aliasing effect, and a finite number of samples N is used for the Fourier

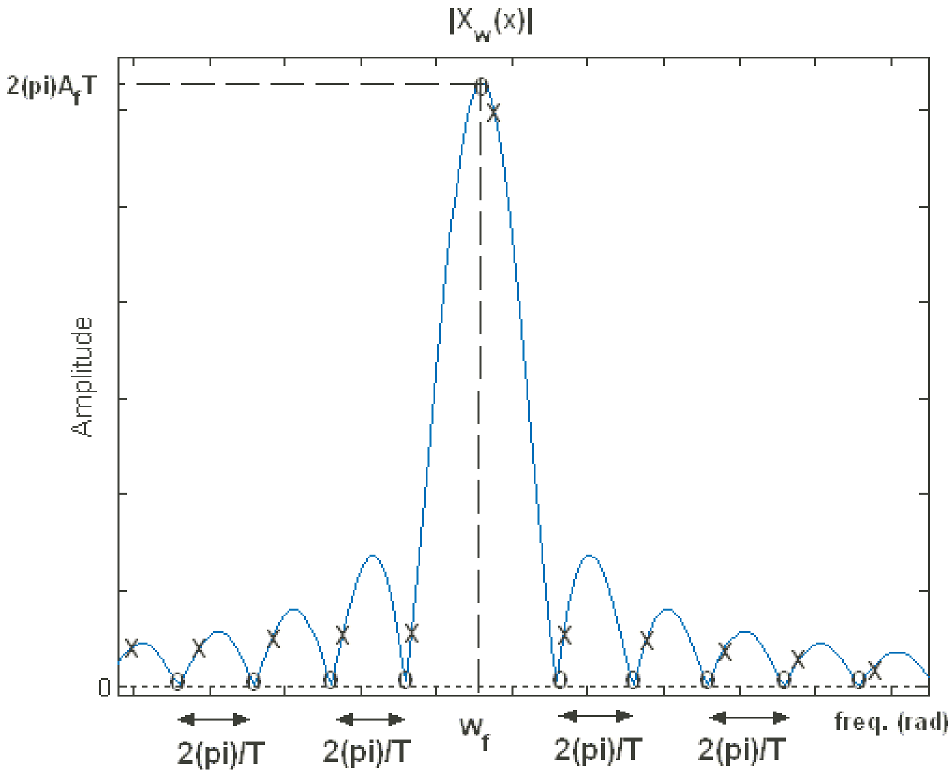

Figure 2.8: Amplitude of $X_w(\omega)$. Xs and Os show the frequency samples without and with frequency deviation, respectively [23].

analysis. This corresponds to windowing the signal with a rectangular window, $w[n]$ of duration $T = N/f_s$. In equation (2.20), $W(w)$ is the Fourier transform of this window function, $w[n]$, as given in equation (2.14), $2\pi AT$ is the measured fundamental amplitude from the FFT, w_n is the nominal fundamental frequency (which is $50Hz$ or $60Hz$), A_f is the actual amplitude of the deviated fundamental frequency. Since w_f, $2\pi AT$, and w_n are known, it is possible to solve for A_f. The FFT window is adjusted to have zero-phase at the fundamental frequency f_f. Therefore, the synthetic signal $v_s[n]$, which has zero phase, represents the fundamental component of $v[n]$ exactly. Then the discrete-time Fourier transform of $v_s[n]$ is obtained, which is denoted by $V_s[k]$ in Figure 2.6. $V_s[k]$ contains a single frequency, therefore the non-zero frequency components around the fundamental component show the effect of the leakage, which corresponds to the first term in (2.19). In the ideal case of $f_f = 50Hz$, all FFT amplitudes except the $50Hz$ component should be equal to zero. On the other hand, when the fundamental frequency deviates, FFT amplitudes in the neighborhood of $50Hz$ component are non-zero. Therefore, these synthetic amplitudes are used to correct the amplitudes of the FFT of the actual voltage waveform, $V[k]$, around the fundamental frequency, which are $f - f_{fi}$ to $f + f_{fi}$ (from $25Hz$ to $75Hz$ for the $50Hz$ case), where f is the nominal frequency. It has been shown in the previous subsection that the leakage effect due to the fundamental frequency shift is additive, therefore, the correction is applied so as to subtract the leakage effect obtained from the FFT of the synthetic sine wave, $V_s[k]$, from the FFT of the original voltage, $V[k]$. A vector subtraction is applied individually on each of the FFT components from $f - f_{fi}$ to $f + f_{fi}$ except the fundamental, which is $50Hz$ or $60Hz$. The corrected spectrum is denoted by $V_c[k]$, and the instantaneous flicker sensation, S, is computed from this corrected spectrum.

FFT amplitudes and the phases from an example voltage waveform which is $200ms$ long and obtained from the secondary of the EAF transformer at an EAF plant are shown in Figure 2.9. The fundamental frequency of this waveform is detected as $50.0336Hz$. The FFT amplitudes around the fundamental frequency of the original and the synthetic waveforms are given in Figure 2.9 (a) and (b), respectively. The phases are given in (c) and (d), and the corrected amplitudes are given in (e). Figure 2.10 shows an example of the vector subtraction for the $55Hz$ component given in Figure 2.9 to obtain the corrected FFT amplitude at $55Hz$. This procedure is repeated for each frequency from $f-25Hz$ to $f+25Hz$ except for the fundamental frequency.

The results with the spectral correction are given in Table 2.2 under the column "*With Spectral Correction*". It is observed that without spectral correction huge errors can be observed, especially in P_{st} values, when the fundamental frequency deviates. The proposed spectral correction, on the other hand, provides unity instantaneous flicker sensation within a 1% tolerance band.

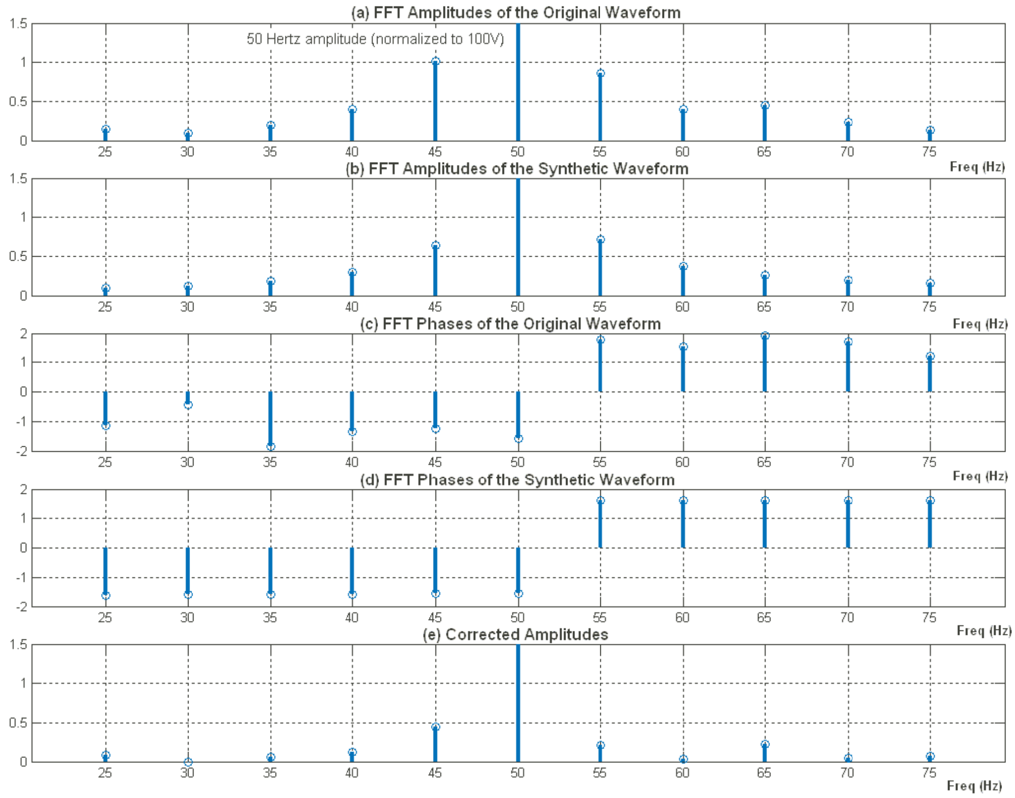

Figure 2.9: Spectral amplitude correction.

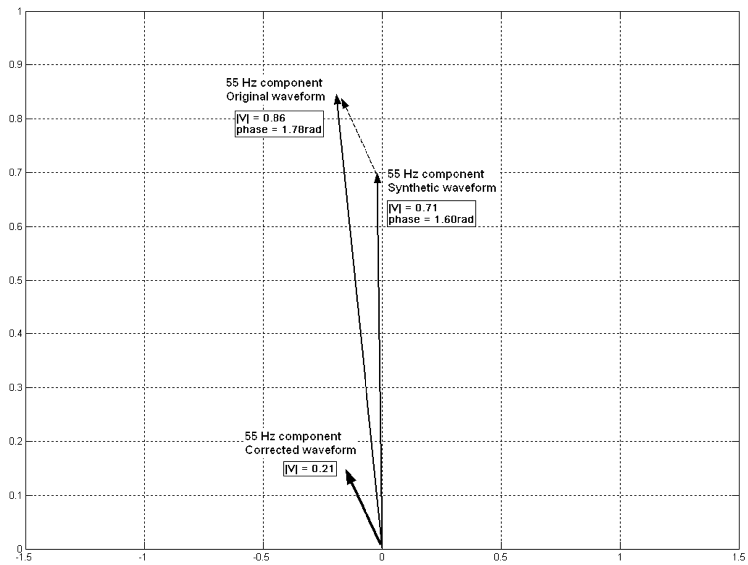

Figure 2.10: Amplitude correction of the $55Hz$ component in Figure 2.9. Correction is achieved by vector subtraction of the synthetic component from the original component using both phases and amplitudes given in Figure 2.9.

To demonstrate the usefulness of the proposed spectral correction method, an example instantaneous flicker sensation computation is given in Figure 2.11 with and without spectral correction applied on the 10-minute duration voltage obtained at the MV side of an AC EAF plant. The frequency deviation is also given in Figure 2.11 (a) to illustrate the increase in the error due to the FFT leakage when the frequency deviates more from the $50Hz$ value between minutes 3.5 and 6. Figure 2.11 (b) shows S computed without the spectral correction compared with the S obtained from the digital realization of the IEC flickermeter. In part (c), S computed with spectral correction is given. It is observed that spectral correction helps to estimate S very close to the IEC result especially when the frequency deviation is significant.

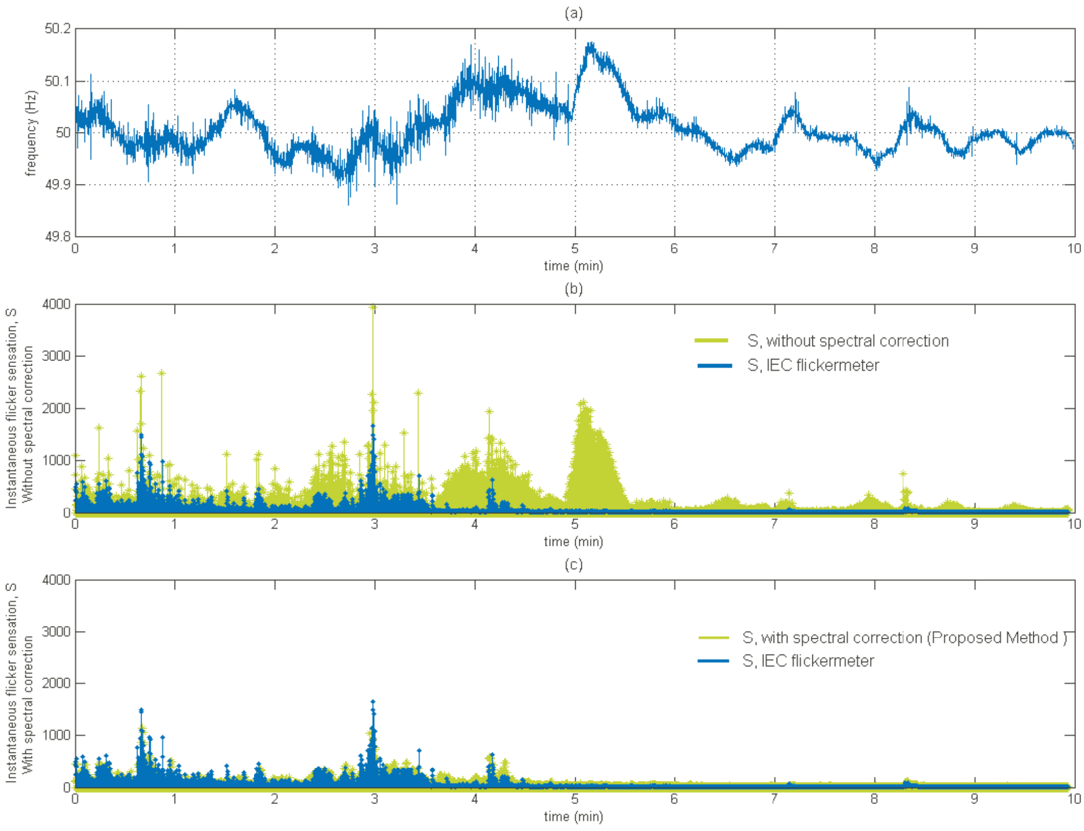

Figure 2.11: Effect of frequency variation on estimation of S. (a) Frequency variation, (b) estimation of S without spectral correction compared with the IEC flickermeter result, (c) estimation of S with the proposed method (with spectral correction) compared with the IEC flickermeter result.

2.4 Verification of the Proposed Method

For verification of the proposed method, a digital realization of the IEC flickermeter given in [9] is used to compare the response of the proposed method to the actual IEC flickermeter behavior. Both simulated and field data are used in order to test the proposed method.

2.4.1 Verification with Simulated Data

Simulated data is produced by modulating the sine wave at $50Hz$ system frequency as given in (2.1) with various flicker frequencies and the corresponding $\Delta V/V$ values in Table 2.1 with a sampling frequency of $3200Hz$. Data length is selected as 10 minutes. S is computed with the proposed light flicker estimation method and the digital IEC flickermeter realization and the results are compared. Three tests are done to test the proposed algorithm with simulated data.

2.4.1.1 Test 1: Single Flicker Frequency Case

A single sinusoidal flicker frequency case is given in (2.1). It is expected that S should be close to unity since Table 2.1 given in the IEC standard [1] is for unity S response to sinusoidal voltage fluctuations. The experiment is repeated with FFT window sizes of both $200ms$ and $2s$ (corresponding to 10 cycles and 100 cycles of the ideal system frequency), resulting in an FFT frequency resolution of $5Hz$ and $0.5Hz$ respectively. In fact, $2s$ is a long time for the actual EAF voltage to be stationary and the recommended window size is $200ms$ according to [16]; however, in case of simulated signals, data can be kept stationary as long as required, so both resolutions are used to test the algorithm. In case of $0.5Hz$ resolution, summation of all S_i given in (2.11) from $0.5Hz$ to $25Hz$ are used to obtain S, whereas $\Delta V/V$ values corresponding to only $5, 10, 15, 20$ and $25Hz$ are added up to obtain S in case of $5Hz$ resolution. Comparison of the results with those of the IEC flickermeter are given in Table 2.3 for both resolution values.

Table 2.3: Proposed light flicker estimation algorithm response for sinusoidal voltage fluctuations

Input voltage fluctuation to obtain $S = 1$ with IEC flickermeter		Proposed flickermeter response			
		$5Hz$ resolution		$0.5Hz$ resolution	
flicker freq.(Hz)	$\Delta V/V\%$	S	error(%)	S	error(%)
5.0	0.40	1.00	0.0	1.00	0.0
10.0	0.26	1.00	0.0	1.00	0.0
12.0	0.31	1.01	1.0	1.00	0.0
15.0	0.43	1.00	0.0	1.00	0.0
20.0	0.70	1.00	0.0	1.00	0.0
25.0	1.04	1.00	0.0	1.00	0.0

2.4.1.2 Test 2: Rectangular Voltage Fluctuations-Combinations of Flicker Frequencies

Rectangular fluctuation of the voltage is given as

$$v(t) = V sin(2\pi ft) \left\{ 1 + \frac{\Delta V}{2V} signum[sin(2\pi f_f t)] \right\}. \tag{2.21}$$

Rectangular fluctuation can be considered as the linear combination of odd harmonic sinusoidal fluctuations due the Fourier Series expansion of the rectangular periodic waveform. This corresponds to representing the rectangular fluctuations as given in (2.2). Normalized flickermeter response for rectangular voltage fluctuations is also tabulated in [1]. To test the proposed method, simulated waveform in (2.21) is obtained with $\Delta V/V$ values taken from the Table "*Normalized flickermeter response for rectangular fluctuations*" for $230V$ lamp and $50Hz$ systems in the IEC Standard [1]. This table is provided in Appendix A, Table A.1. It is observed that the proposed method estimates S with a maximum error of 6% as given in Table 2.4.

2.4.1.3 Test 3: Homogeneity of the Flickermeter Response

The Standard IEC-61000-4-15 requires that the flickermeter response should have the homogeneity property, i.e., whenever the $\Delta V/V$ value is doubled, the resulting flicker severity P_{st} should also be doubled [1]. Homogeneity of the proposed algorithm is checked by applying twice as much and half of the $\Delta V/V$

Table 2.4: Proposed flicker estimation algorithm response for rectangular voltage fluctuations

Input voltage fluctuation to obtain $S=1$ with IEC flickermeter		Proposed flickermeter response			
		$5Hz$ resolution		$0.5Hz$ resolution	
flicker freq.(Hz)	$\Delta V/V\%$	S	error(%)	S	error(%)
5.0	0.29	0.98	-2.0	0.98	-2.0
10.0	0.21	1.03	3.0	1.04	4.0
12.0	0.25	1.02	2.0	1.02	2.0
15.0	0.34	1.04	4.0	1.06	6.0
20.0	0.55	0.99	-1.0	1.02	2.0

values with the corresponding flicker frequencies given in Table 2.1. If the homogeneity of the proposed algorithm holds, it is expected that P_{st} value is doubled and halved, when $\Delta V/V$ is doubled and halved, respectively. It is observed that the proposed method estimates P_{st} values with minor error as given in Table 2.5. The error in this table is defined as the percentage difference between twice/half of the P_{st} computed by the IEC flickermeter and the P_{st} obtained by the proposed method when $\Delta V/V$ is doubled/halved.

2.4.2 Verification on AC Arc Furnace Data

To verify the effectiveness of the proposed algorithm in estimating the light flicker, experiments on field data obtained at three different EAF plants are used. The proposed light flicker estimation algorithm is used with $5Hz$ frequency resolution ($200ms$ windows). The data is obtained during field measurements carried out through the National Power Quality Project of Turkey [22, 26]. EAF voltages are collected at a sampling rate of $3200Hz$ [25]. EAF rms voltages obtained at the MV side of the EAF transformer at three plants are given with the instantaneous flicker sensation, S, values obtained from both the digital implementation of the IEC flickermeter and the proposed light flicker estimation algorithm in Figures 2.12, 2.13, and 2.14. In these figures, (a) shows the rms voltages with the P_{st} computed intervals, (b) shows the frequency variation, and (c) shows S computed with both the proposed method and the IEC flickermeter for comparison. It is observed that the proposed method gives good estimates

Table 2.5: Homogeneity of the proposed light flicker estimation algorithm

Flicker frequency (Hz) sinusoidal fluctuation	$\Delta V/V\%$ 230V/50Hz system	P_{st}	% Error
0.5	2.340	0.98	–
	2×2.340	1.96	0.00
	0.5×2.340	0.49	0.00
2.5	0.754	0.59	–
	2×0.754	1.17	+0.84
	0.5×0.754	0.30	-1.67
5.0	0.398	0.69	–
	2×0.398	1.38	0.00
	0.5×0.398	0.35	-1.45
10.0	0.260	0.69	–
	2×0.260	1.38	0.00
	0.5×0.260	0.35	-1.45
12	0.312	0.73	–
	2×0.312	1.46	0.00
	0.5×0.312	0.37	0.00
15	0.432	0.69	–
	2×0.432	1.38	0.00
	0.5×0.432	0.35	-1.45
18	0.584	0.78	–
	2×0.584	1.55	+0.64
	0.5×0.584	0.39	0.00
20	0.700	0.69	–
	2×0.700	1.38	0.00
	0.5×0.700	0.35	-1.45
25	1.042	0.69	–
	2×1.042	1.38	0.00
	0.5×1.042	0.35	-1.45

of the instantaneous flicker sensation, S. More detailed views of S for the first two intervals for Figures 2.12, 2.13, and 2.14 are given in Figures 2.15, 2.16, and 2.17, respectively for a better comparison. To give a quantitative comparison of the algorithm, short term flicker severity, P_{st}, is computed for the intervals given in the figures and the results are compared with the results of the digital realization of the IEC flickermeter as given in Tables 2.6, 2.7 and 2.8. The results indicate good agreement between the IEC flickermeter and the proposed method.

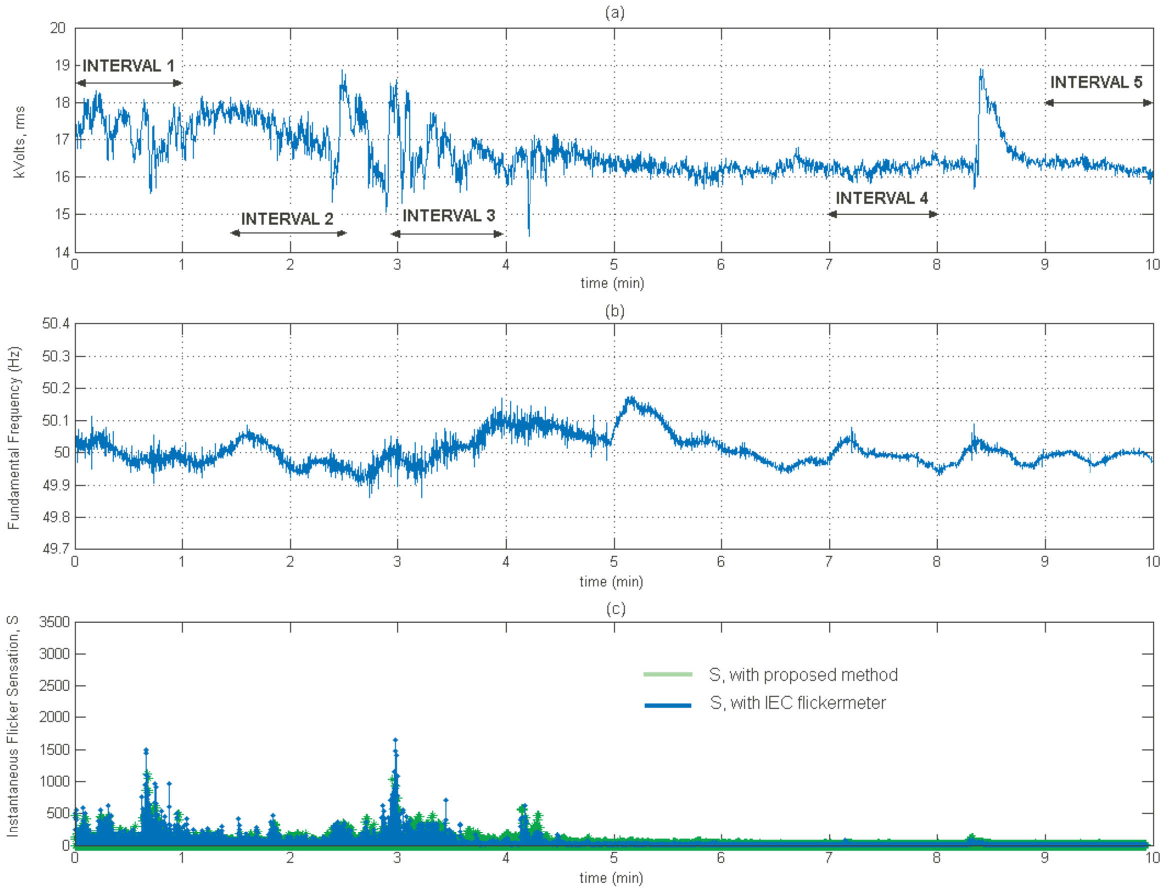

Figure 2.12: Plant-1 (a) rms voltage at the MV side of the EAF Plant with the P_{st} computed intervals, (b) fundamental frequency variation, (c) instantaneous flicker sensation, S.

Table 2.6: Short term flicker severity, P_{st}, computed inside the intervals given in Fig 2.12 with the proposed method and the digital realization of the IEC flickermeter

	INTERVAL 1	INTERVAL 2	INTERVAL 3	INTERVAL 4	INTERVAL 5
IEC Flickermeter	15.4958	9.5497	13.2904	2.6938	1.8163
Proposed Method	15.4131	9.6166	13.5436	2.6922	1.9905
Error %	+0.53	-0.70	-1.91	+0.06	-9.59

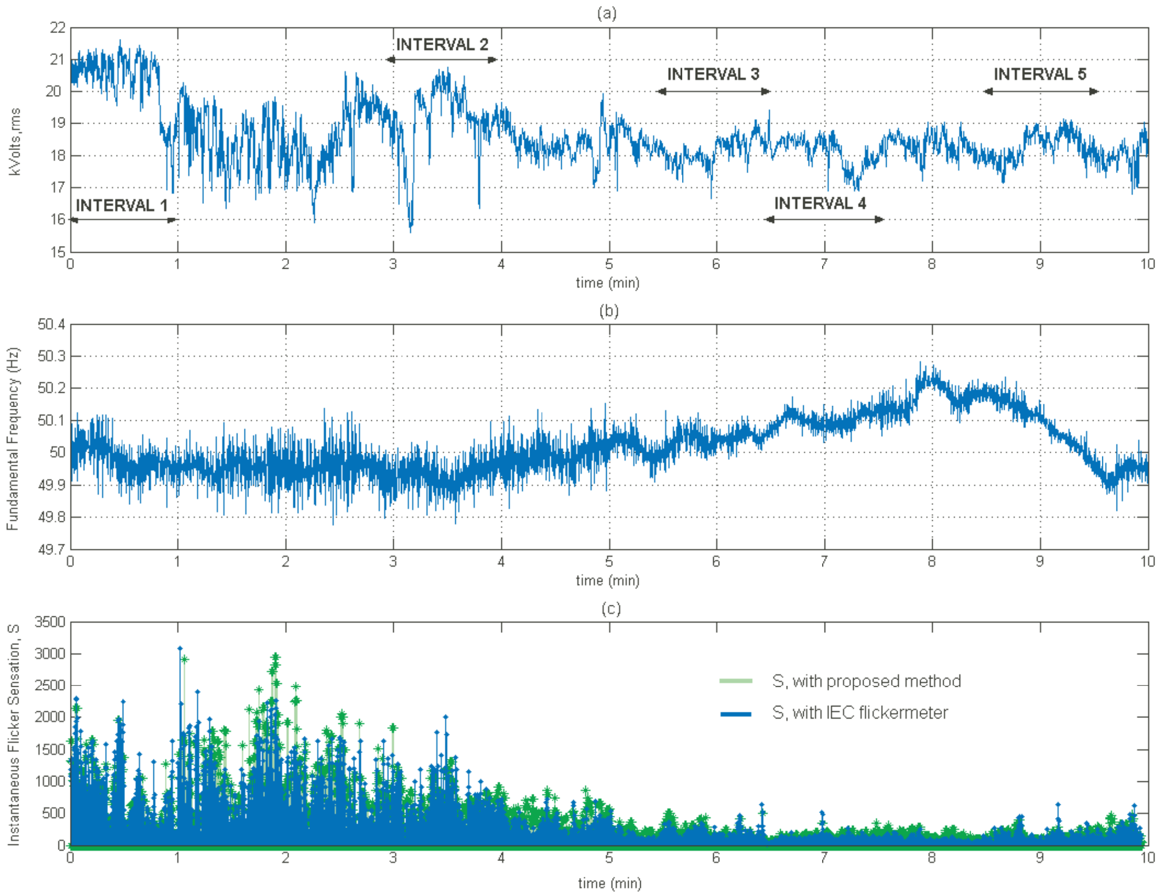

Figure 2.13: Plant-2 (a) rms voltage at the MV side of the EAF Plant with the P_{st} computed intervals, (b) fundamental frequency variation, (c) instantaneous flicker sensation, S.

Table 2.7: Short term flicker severity, P_{st}, computed inside the intervals given in Figure 2.13 with the proposed method and the digital realization of the IEC flickermeter

	INTERVAL 1	INTERVAL 2	INTERVAL 3	INTERVAL 4	INTERVAL 5
IEC Flickermeter	22.3209	21.4275	11.5852	9.2761	10.6356
Proposed Method	23.3268	22.5856	11.9070	9.4001	10.9129
Error %	-4.51	-5.40	-2.78	-1.34	-2.61

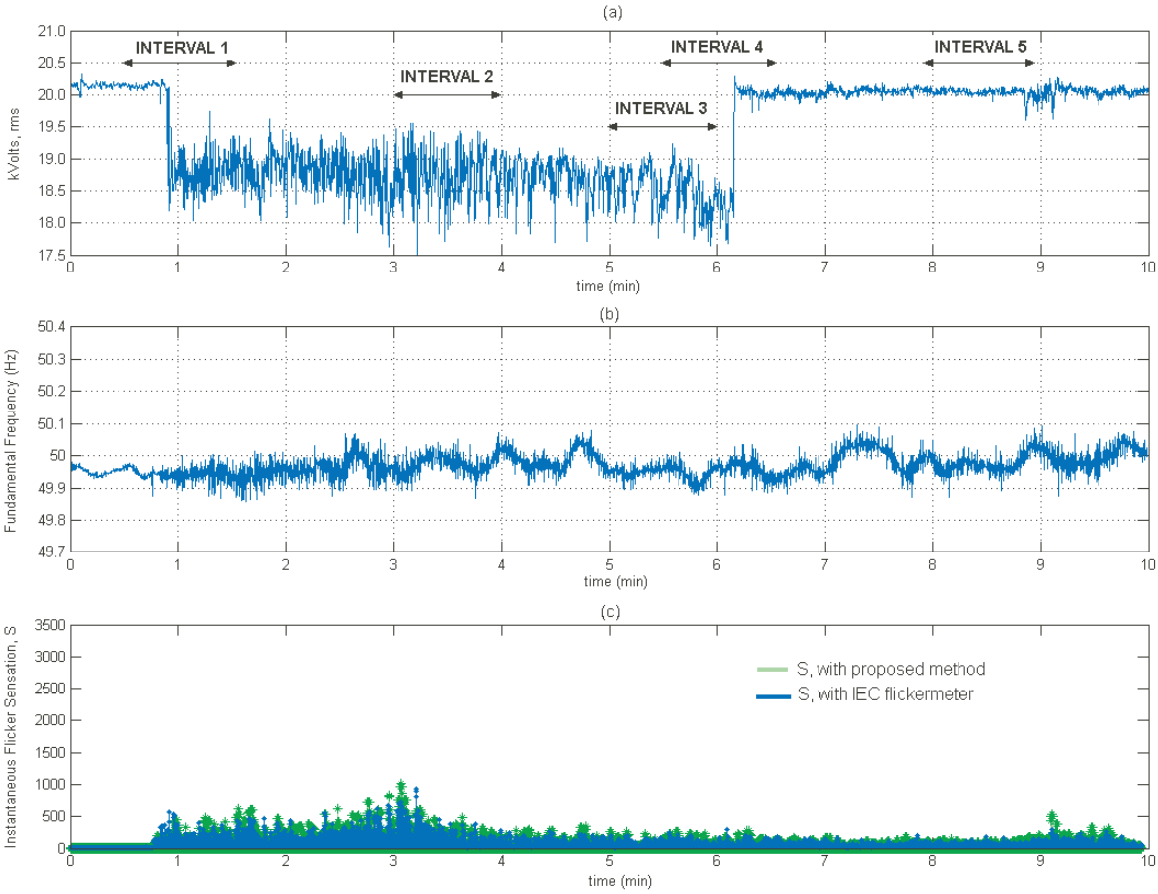

Figure 2.14: Plant-3 (a) rms voltage at the MV side of the EAF Plant with the P_{st} computed intervals, (b) fundamental frequency variation, (c) instantaneous flicker sensation, S.

Table 2.8: Short term flicker severity, P_{st}, computed inside the intervals given in Figure 2.14 with the proposed method and the digital realization of the IEC flickermeter

	INTERVAL 1	INTERVAL 2	INTERVAL 3	INTERVAL 4	INTERVAL 5
IEC Flickermeter	11.6423	16.0384	9.0006	8.2767	6.4816
Proposed Method	11.7285	15.6946	9.2464	8.8416	7.4208
Error %	-0.74	+2.14	-2.73	-6.83	-14.49

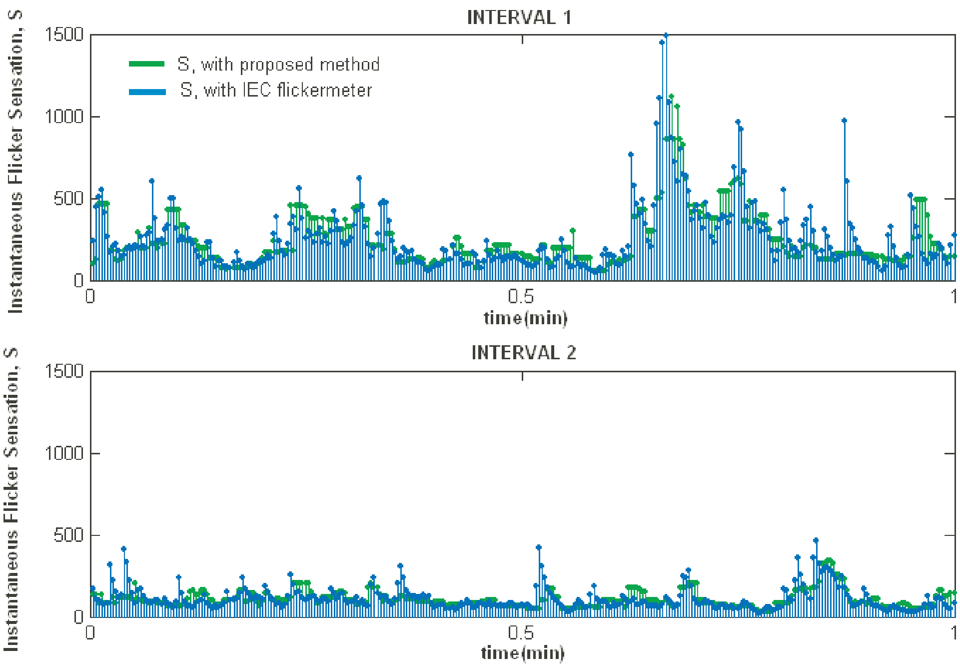

Figure 2.15: Plant-1 instantaneous flicker sensation, S, for Interval-1 and Interval-2 in Figure 2.12 for a more detailed comparison of the proposed method and the IEC flickermeter.

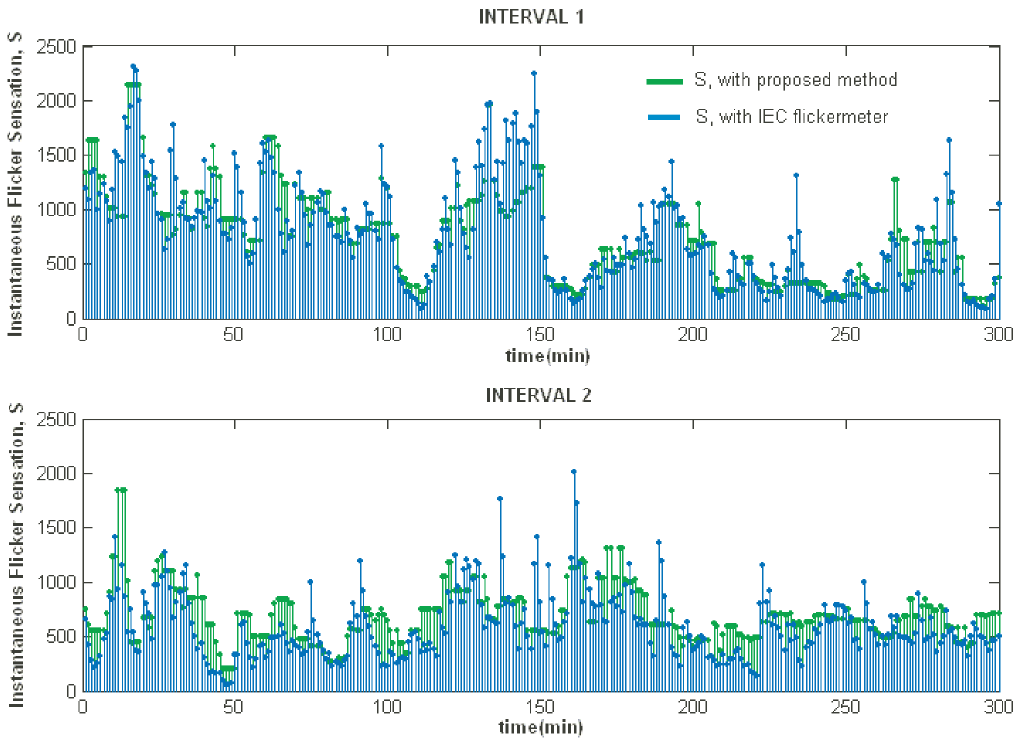

Figure 2.16: Plant-2 instantaneous flicker sensation, S, for Interval-1 and Interval-2 in Figure 2.13 for a more detailed comparison of the proposed method and the IEC flickermeter.

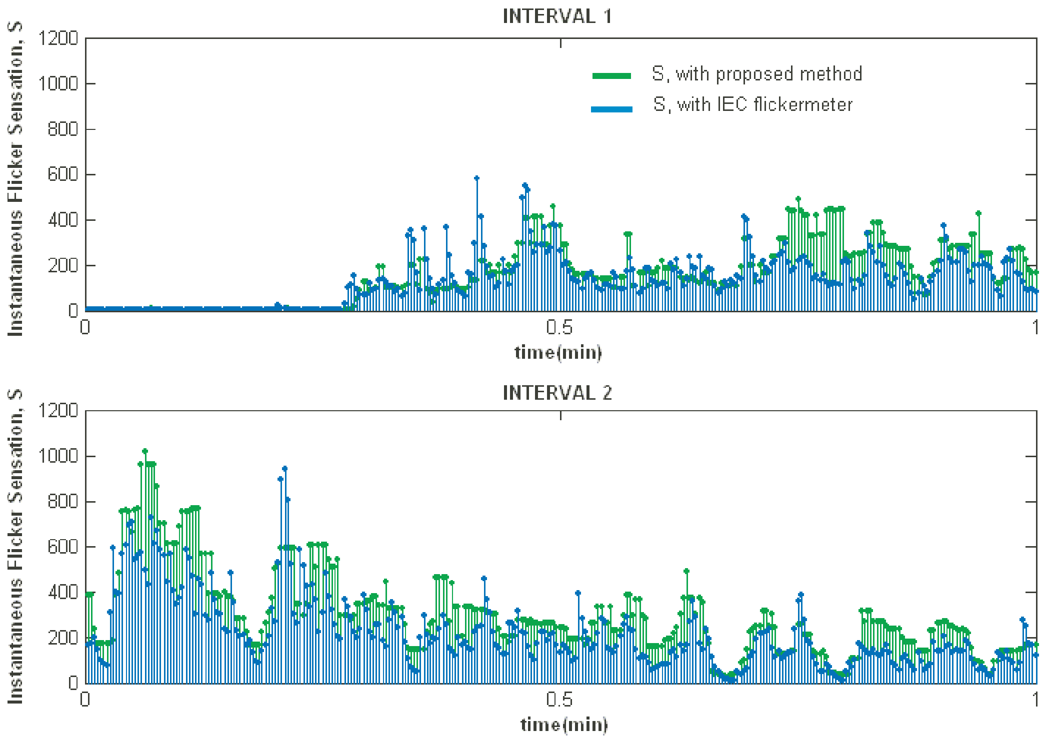

Figure 2.17: Plant-3 instantaneous flicker sensation, S, for Interval-1 and Interval-2 in Figure 2.14 for a more detailed comparison of the proposed method and the IEC flickermeter.

The calculation procedures are analyzed on a personal computer (PentiumIV, $2.20GHz$). All algorithms are implemented using MATLAB running on Windows XP. The total computation time for a $10min$ input data is $3.5s$. This shows the computational efficiency of the method when compared with the computation times given in [2], which are inside the range from $7.96s$ to $0.91s$ for an input data length of $4s$ with MATLAB running on a PentiumIV, $2.20GHz$ personal computer.

The accuracy obtained on field data are comparable with the results given in [5] and in [2]. The mean error is 2.56%, 3.33%, and 5.39% for Plant-1, Plant-2 and Plant-3, respectively. In [2], mean error is around 6% and it varies between 0.44% and 5.94% in [5], which shows that the proposed method gives satisfactory results.

For a more detailed comparison, also the method proposed in [5] is compared with the proposed method in this research work. Initially the method in [5] is implemented and the data given in Figure 2.12 are used to compare the P_{st}

results of the two methods. Table 2.9 presents the results. It is shown that the proposed method provides comparable results with the methods presented in the literature, which shows that the method is successful in estimating the light flicker.

Table 2.9: Comparison of the short term flicker severity, P_{st}, computed inside the intervals given in Fig 2.12 with the proposed method, the method given in [5] and the digital realization of the IEC flickermeter

	INTERVAL 1	INTERVAL 2	INTERVAL 3	INTERVAL 4	INTERVAL 5
Error % (Method in [5])	+1.81	-3.72	-1.92	+0.08	-8.86
Error % (Proposed Method)	+0.53	-0.70	-1.91	+0.06	-9.59

CHAPTER 3

A KALMAN FILTERING BASED APPROACH FOR LIGHT FLICKER EVALUATION OF POWER SYSTEMS

Flicker evaluation method based on interharmonic spectrum is provided in detail in Chapter 2 and in [7]. It has been shown that the effect of each interharmonic frequency, f_{fi}, to the instantaneous flicker sensation S is

$$S_i = \frac{\frac{V^4}{8}\left(\frac{\Delta V_i}{V}\right)^2 H^2(f_{fi})}{\frac{V^4}{8}\left(\frac{\Delta V_i}{V}\right)^2_{IEC} H^2(f_{fi})} = \frac{\left(\frac{\Delta V_i}{V}\right)^2}{\left(\frac{\Delta V_i}{V}\right)^2_{IEC}} \tag{3.1}$$

and S is obtained as the summation of all S_i, $S = \sum_{i=1}^{N} S_i$, where f_{fi} varies from $5Hz$ to $25Hz$ with $5Hz$ increments for 10-cycle windows.

In the method presented in this chapter, the frequency domain components of the voltage waveform are obtained by Kalman filtering and these components are used to obtain the light flicker using the relationship given in (3.1). In order to describe the usage of the Kalman filters in the proposed method, the general characteristic of Kalman filters is explained in Section 3.1 based on [27].

3.1 General Characteristics of Kalman Filters

The Kalman filter is a set of mathematical equations. It provides an efficient recursive algorithm to estimate the state of a process, by minimizing the mean of the squared error. The Kalman filter supports estimations of past, present, and even future states. It can achieve success even when the precise nature of the modeled system is unknown.

As it is clearly explained in [27], the aim of the Kalman filter is to estimate the state variable $x \in R^n$ of a discrete time controlled process which is shown by the linear stochastic difference equation

$$x_k = Ax_{k-1} + Bu_{k-1} + w_{k-1} \tag{3.2}$$

with a measurement $z \in R^m$ which is shown as

$$z_k = Hx_k + v_k \tag{3.3}$$

The random variable w_k represents the process noise and the random variable v_k represents the measurement noise which are assumed to be independent from each other, white and with normal probability distributions. The process noise covariance is represented by Q, and the measurement noise covariance is represented by R.

The aim of the n x n matrix A in (3.2) is to relate the state at the previous time step $k-1$ to the state at the current step k. The aim of the n x l matrix B in (3.2) is to relate the optional control input $u \in R^l$ to the state x. In (3.3), the m x n matrix H relates the state to the measurement z_k.

Initially a priori state estimate at step k, $\hat{x}_k^- \in R^n$, and a posteriori state estimate at step k, $\hat{x}_k \in R^n$, are defined with given measurement z_k. Then a priori and posteriori estimate errors are defined as

$$e_k^- = x_k - \hat{x}_k^- \tag{3.4}$$

and

$$e_k = x_k - \hat{x}_k \tag{3.5}$$

$P_k^- = E[e_k^- {e_k^-}^T]$ is then called as a priori estimate error covariance and $P_k = E[e_k {e_k}^T]$ is called as a posteriori estimate error covariance.

At each iteration the estimate of the state variable is updated with measurement z_k as given below.

$$\hat{x}_k = \hat{x}_k^- + K(z_k - H\hat{x}_k^-) \tag{3.6}$$

In (3.6), $H\hat{x}_k^-$ is the predicted measurement and z_k is the actual measurement. The difference $(z_k - H\hat{x}_k^-)$ is called the residual which shows the discrepancy between the predicted and the actual measurements. In this equation, the n x m matrix K is the gain, which minimizes the posteriori error covariance, P_k. One form of the resulting K, which minimizes P_k is given as

$$K_k = P_k^- H^T (H P_k^- H^T + R)^{-1}. \tag{3.7}$$

Using these new parameters, the linear Kalman filter is implemented as explained below.

The Kalman filter estimates a process by using a form of feedback control. Therefore, the equations for the Kalman filter fall into two groups. First group consists of *time update* equations and second group consists of *measurement update* equations. The time update equations are responsible for projecting forward the current state and error covariance estimates in order to obtain a priori estimates for the next time step [27]. On the other hand, the measurement update equations are responsible for the feedback part. This part incorporates a new measurement into the a priori estimate to obtain an improved a posteriori estimate [27]. Therefore, it is possible to declare that time update equations are responsible for prediction whereas measurement update equations are responsible for the correction.

The linear Kalman filter time update equations are given as follows :

$$\hat{x}_k^- = A\hat{x}_{k-1}^- + Bu_{k-1}$$
$$P_k^- = AP_{k-1}A^T + Q$$

while the linear Kalman filter measurement update equations are given as below:

$$K_k = P_k^- H^T (H P_k^- H^T + R)^{-1}$$
$$\hat{x}_k = \hat{x}_k^- + K_k(z_k - H\hat{x}_k^-)$$
$$P_k = (I - K_k H)P_k^-$$

The complete operation of the linear Kalman filter is given in Figure 3.1. Each step of this figure is explained in [27] clearly.

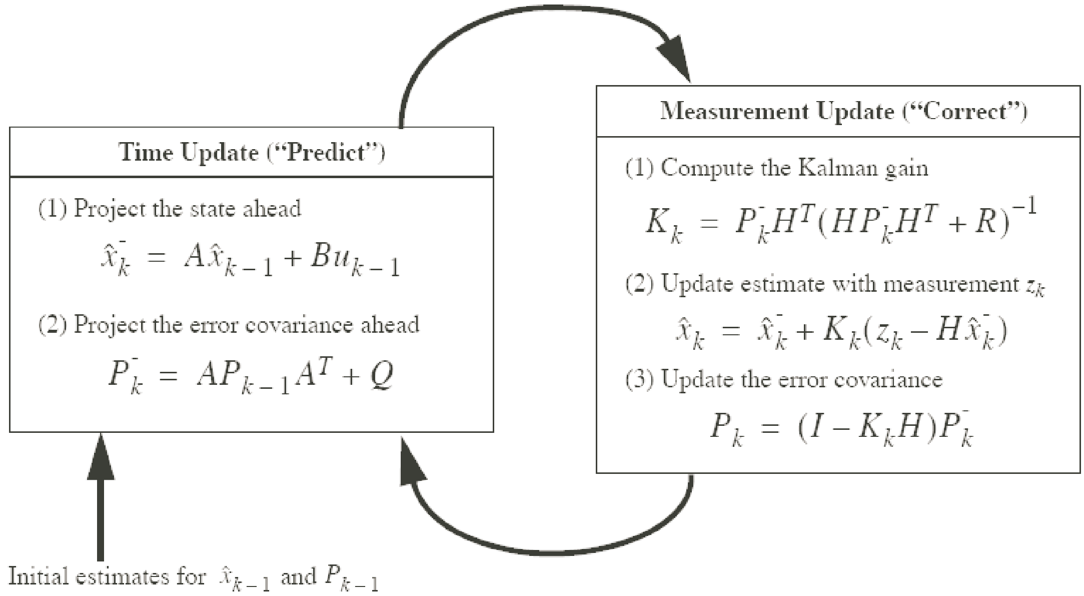

Figure 3.1: Block diagram of the operation of the Kalman Filter [27].

The extended Kalman filter is a little bit different from the linear Kalman filter algorithm. When the process to be estimated and or the measurement relationship to the process is nonlinear, extended Kalman filter is used. Thus, a Kalman filter that linearizes about the current mean and covariance is referred to as an EKF [27].

The extended Kalman filter time update equations are given as follows :

$\hat{x}_k^- = f(\hat{x}_{k-1}^-, u_{k-1}, 0)$
$P_k^- = A_k P_{k-1} {A_k}^T + W_k Q_{k-1} {W_k}^T$

while the extended Kalman filter measurement update equations are given as below :

$K_k = P_k^- {H_k}^T (H_k P_k^- Hk^T + V_k R_k {V_k}^T)^{-1}$
$\hat{x}_k = \hat{x}_k^- + K_k(z_k - h(\hat{x}_k^-, 0))$
$P_k = (I - K_k H_k)P_k^-$

Figure 3.2 shows the complete operation of the extended Kalman filter. The detailed explanation of the steps of the EKF algorithm is included in [27].

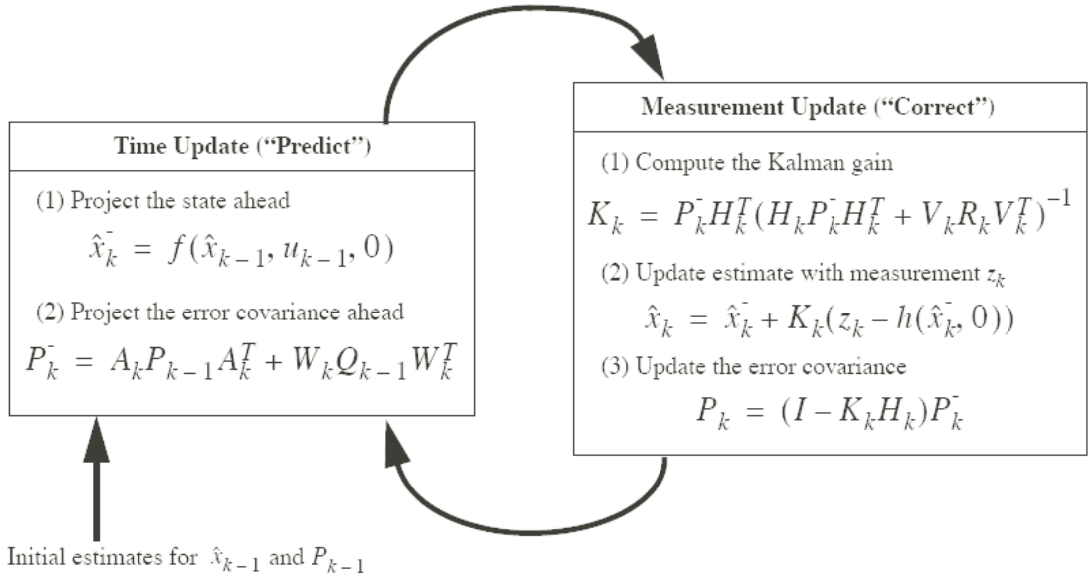

Figure 3.2: Block diagram of the operation of the Extended Kalman Filter [27].

In the proposed method, an EKF is used to estimate the voltage envelope and then a LKF is used to obtain the spectral amplitudes out of the voltage envelope causing light flicker.

3.2 Obtaining the Spectral Decomposition based on Kalman Filtering

The block diagram of the proposed spectral decomposition algorithm, which is also explained in [18], is given in Figure 3.3. To obtain spectral decomposition by Kalman filtering, a standard window length is used. When the fundamental frequency deviates from the nominal value, the window size is not an integer multiple of the actual cycle any more. In such a case, when DFT algorithm is used to obtain the spectral decomposition, even in a very small deviation of the fundamental frequency case, leakage effect occurs on the DFT components, which causes significant error as explained in detail in Section 2.3. However, in the proposed spectral decomposition method, fundamental frequency deviation is not so critical in terms of the estimated spectral amplitudes. Since Kalman filters are used to obtain the spectral decomposition, no leakage effect problem occurs.

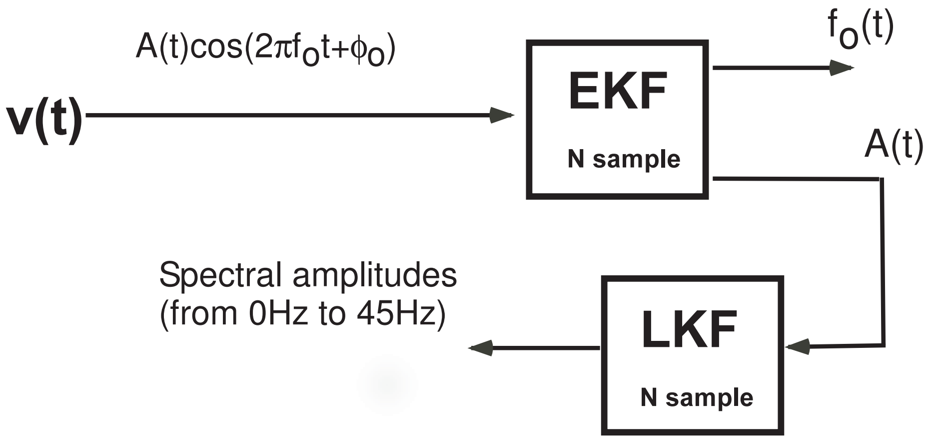

Figure 3.3: Block diagram of the proposed spectral decomposition method.

In the proposed method, window length is selected as $200ms$, which is the recommended window length in the harmonic and interharmonic computation standard of IEC, IEC-61000-4-7 [16]. Then for each time window of $200ms$, the spectral decomposition is obtained by applying two types of Kalman filters, EKF and LKF, consecutively [18, 19]. The EKF and LKF algorithms are implemented based on [27]. The voltage fluctuation containing interharmonic frequencies around the fundamental frequency can be modeled as given in [1]

$$v(t) = cos(2\pi f_o t + \phi_o)\left\{V + \sum_{i=1}^{N} \frac{\Delta V_i}{2} cos(2\pi f_i t + \phi_i)\right\}. \tag{3.8}$$

The voltage signal in (3.8) represents the voltage fluctuation especially observed in EAF plants, which contains several interharmonic frequencies. Figure 3.4 shows an example voltage waveform containing several interharmonic frequencies. As it is clearly seen from this figure that the signal model in (3.8) can also be modeled as a sinusoidal voltage waveform with time varying amplitude $A(t)$ and it is shown as

$$\begin{aligned} v(t) &= A(t)cos(2\pi f_o t + \phi_o), \\ &= A(t)cos(\phi_o)cos(2\pi f_o t) - A(t)sin(\phi_o)sin(2\pi f_o t). \end{aligned} \tag{3.9}$$

In equation (3.9), $A(t)$ is the envelope of the input signal which can also be defined as the time varying amplitude of the input signal. To obtain the spectral decomposition of the input signal, $v(t)$, first the voltage envelope, $A(t)$ is

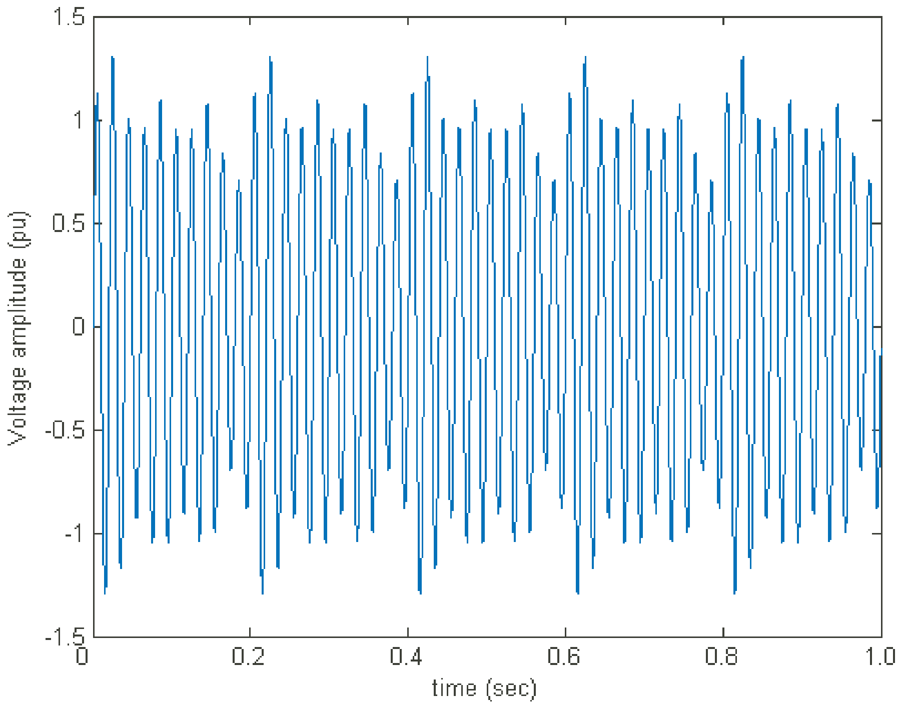

Figure 3.4: Voltage waveform containing different interharmonic frequencies.

obtained by applying an EKF on the waveform [18]. $A(t)$ is assumed to contain N frequency components, which cause interharmonics around the fundamental. In the second step of the proposed algorithm, these frequency components are determined by applying a LKF as shown in the block diagram of the proposed method, Figure 3.3.

Kalman filters are used to estimate the state $x \in R^n$ of a discrete time controlled process which is governed by a linear stochastic difference equation as shown as

$$x_k = Ax_{k-1} + Bu_{k-1} + w_{k-1} \tag{3.10}$$

with a measurement $z \in R^m$, which is shown as

$$z_k = Hx_k + v_k. \tag{3.11}$$

The random variable w_k represents the process noise and the random variable v_k represents the measurement noise, which are assumed to be independent from each other, white and with normal probability distributions. However, when the process to be estimated or when the measurement relationship to the process is nonlinear, extended Kalman filters are used as mentioned in the previous Section 3.1. In the proposed method, EKF is used to obtain the envelope, $A(t)$, therefore the state variables for this EKF algorithm are determined as given below :

x_1 : in-phase component of $v(t)$, $(A(t)cos(\phi_o))$,

x_2 : quadrature-phase component of $v(t)$, $(A(t)sin(\phi_o))$,

x_3 : fundamental frequency of $v(t)$, (f_o).

The EKF is applied on the voltage waveform for N sample windows as shown in Figure 3.3. Since in the proposed method a standard window length of $200ms$ is used as recommended in the standard IEC-61000-4-7 [16], each window consists of $0.2*f_s$ samples, where f_s is the number of samples per second. For verification of the proposed method, all tests are achieved with a sampling frequency of $3.2kHz$, which means that EKF is applied on the windows of length 640 samples. For each time step, the voltage phasor, which is represented by x_1+jx_2, is rotated by the amount of $2\pi x_3\Delta t$. The state transition of x_1 and x_2 can be written as ;

$$x_1(k+1) + jx_2(k+1) = [x_1(k) + jx_2(k)]e^{j2\pi x_3(k)\Delta t}. \tag{3.12}$$

According to the equation (3.12), the nonlinear state transition equation is obtained as

$$\begin{bmatrix} x_1(k+1) \\ x_2(k+1) \\ x_3(k+1) \end{bmatrix} = \begin{bmatrix} x_1(k)cos(2\pi x_3(k)\Delta t) - x_2(k)sin(2\pi x_3(k)\Delta t) \\ x_1(k)sin(2\pi x_3(k)\Delta t) - x_2(k)cos(2\pi x_3(k)\Delta t) \\ x_3(k) \end{bmatrix}. \tag{3.13}$$

Since the fundamental frequency observed in the power systems is not usually constant in practice, it is also considered as the state variable, x_3, to be estimated in the proposed method. The results show that the proposed method is successful in estimating the fundamental frequency of the voltage waveform. The advantage of the proposed method is that there is no fundamental frequency computation requirement, but it is only determined as a state variable in the EKF algorithm.

The EKF equations in the proposed method are implemented according to [27]. Since the voltage signal is a nonlinear function of the frequency, the state transition and the measurement equations are also nonlinear functions of x_3. In EKF algorithm state transition and measurement equations are combined together in accordance with the EKF model explained in [28]. The EKF model is realized, and by applying EKF on the voltage waveform, its envelope, $A(t)$, is obtained. The linearized state transition matrix and the linearized measurement vector are given as,

$$\Phi = \begin{bmatrix} cos(2\pi\hat{x}_3^-\Delta t) & -sin(2\pi\hat{x}_3^-\Delta t) & 2\pi\Delta t(-\hat{x}_1^- sin(2\pi\hat{x}_3^-\Delta t) - \hat{x}_2^- cos(2\pi\hat{x}_3^-\Delta t)) \\ sin(2\pi\hat{x}_3^-\Delta t) & cos(2\pi\hat{x}_3^-\Delta t) & 2\pi\Delta t(\hat{x}_1^- cos(2\pi\hat{x}_3^-\Delta t) - \hat{x}_2^- sin(2\pi\hat{x}_3^-\Delta t)) \\ 0 & 0 & 1 \end{bmatrix}, \quad (3.14)$$

and

$$H = \begin{bmatrix} cos(2\pi\hat{x}_3^-\Delta t) & sin(2\pi\hat{x}_3^-\Delta t) & 2\pi\Delta t(-\hat{x}_1^- sin(2\pi\hat{x}_3^-\Delta t) + \hat{x}_2^- cos(2\pi\hat{x}_3^-\Delta t)) \end{bmatrix}, \quad (3.15)$$

respectively, where $\hat{x}_i^-$ is a priori state estimate of the i^{th} state.

The EKF algorithm is applied by using the linearized state transition matrix, Φ, and the linearized measurement vector, H. At the output of the EKF, the state variables of the in-phase component of the voltage envelope, the quadrature-phase component of the voltage envelope, and the state variable showing the fundamental frequency deviation are obtained for each window of $200ms$. Using the estimated state variables of the state vector, which is the output of the EKF algorithm, the envelope of the voltage waveform and the fundamental frequency variation are obtained. The envelope of the voltage waveform is formed by using the state variables x_1 and x_2 as

$$A(t) = \sqrt{\hat{x}_1(t)^2 + \hat{x}_2(t)^2}. \quad (3.16)$$

The variation of the state variable x_3 gives the time-varying fundamental frequency, which is represented as

$$f(t) = \hat{x}_3(t). \quad (3.17)$$

The output of the EKF algorithm gives the fundamental frequency variation and the envelope of the voltage waveform. After the EKF, comes a second Kalman filter, which is a linear Kalman filter (LKF). Spectral decomposition of the voltage waveform is obtained by using this LKF. The input of the LKF is the envelope of the voltage waveform, $A(t)$, which is the output of EKF and contains all the frequency components causing interharmonics around the fundamental. The mathematical representation of the envelope of the voltage waveform, $A(t)$, is

$$A(t) = \left\{ V + \sum_{i=1}^{N} \frac{\Delta V_i}{2} cos(2\pi f_i t + \phi_i) \right\}. \tag{3.18}$$

$A(t)$ is the measurement (z_k in the measurement equation (3.11)) of the LKF algorithm. Spectral decomposition of $A(t)$ which is obtained by using a LKF gives the spectral amplitudes at frequencies f_i, directly. Since the aim is to obtain the spectral amplitudes at the interharmonics around the fundamental, the corresponding frequency region for the frequencies, f_i, is between $0 - 45Hz$. In equation (3.18), constant V is considered as a DC voltage signal. Therefore, $A(t)$ is considered to be represented as the summation of ten sinusoidal voltage fluctuations $(0, 5, 10, 15, \cdots, 45Hz)$, and hence the results are obtained with $5Hz$ resolution in the proposed method. Thereby, the results can be compared with $5Hz$ resolution results of the method which is explained in [23]. Higher frequency resolution can be preferred for more precise estimates, although frequency resolution increase has a cost of increasing the matrix dimensions of the state equations. For one of these sinusoidal voltage fluctuations, the in-phase and the quadrature-phase components, which are determined as the two state variables for the corresponding voltage fluctuation in the LKF model, are obtained from sinusoidal expansion of the voltage fluctuation as

$$\frac{\Delta V_i}{2} cos(2\pi f_i t + \phi_i) = \frac{\Delta V_i}{2} cos(\phi_i) cos(2\pi f_i t) - \frac{\Delta V_i}{2} sin(\phi_i) sin(2\pi f_i t). \tag{3.19}$$

In (3.19), states are defined as follows:
x_1 = in-phase component of the sinusoidal fluctuation $(\frac{\Delta V_i}{2} cos(\phi_i))$,
x_2 = quadrature-phase component of the sinusoidal fluctuation $(\frac{\Delta V_i}{2} sin(\phi_i))$,
$i = 1, 2, \cdots, 10$ represents the frequencies $0, 5, 10, 15, \cdots, 45\ Hz$.

The state vector of the LKF, $\bar{x}_k$, is defined as

$$\bar{x}_k = \begin{bmatrix} x_{1,1} & x_{2,1} & x_{1,2} & x_{2,2} & \cdots & x_{1,10} & x_{2,10} \end{bmatrix}_k^T \tag{3.20}$$

where superscript T defines transpose of the vector given in brackets and,

$x_{1,i}$ = in-phase component of the sinusoidal fluctuation at frequency, f_i
$x_{2,i}$ = quadrature-phase component of the sinusoidal fluctuation at frequency, f_i ($f_i = \{0, 5, 10, 15, 20, \cdots, 45\}$).

Then the state transition equation for the twenty-state Kalman filter model is given as

$$\bar{x}_{k+1} = \begin{bmatrix} 1 & 0 & \cdots & 0 \\ 0 & 1 & \cdots & 0 \\ \vdots & \vdots & \ddots & \vdots \\ 0 & 0 & \cdots & 1 \end{bmatrix} \bar{x}_k + \bar{w}_k. \tag{3.21}$$

Since the state variables $x_{1,i}$ and $x_{2,i}$ represent the in-phase and quadrature-phase components of the voltage phasor at frequency f_i, the measurement equation of the LKF is formed as

$$z_k = \beta \bar{x}_k + v_k, \tag{3.22}$$

where the corresponding measurement vector, β, is

$$\beta = \begin{bmatrix} cos(2\pi f_1 t) & -sin(2\pi f_1 t) & cos(2\pi f_2 t) & -sin(2\pi f_2 t) & \cdots & cos(2\pi f_{10} t) & -sin(2\pi f_{10} t) \end{bmatrix}. \tag{3.23}$$

In this twenty-state LKF model, which is formed by equations (3.21) and (3.22), $\bar{w}_k$ represents the process noise vector and v_k represents the measurement noise vector. The spectral amplitude at frequency f_i is obtained by using the corresponding state variables $x_{1,i}$ and $x_{2,i}$, which are calculated for each time window. The spectral amplitude at frequency f_i for the corresponding time window is determined by,

$$\frac{\Delta V_i}{2} = \sqrt{\hat{x}_{1,i}^2 + \hat{x}_{2,i}^2}. \tag{3.24}$$

3.2.1 Verification of Kalman Filtering Method for Interharmonic Detection

The proposed spectral decomposition method is verified by computations on both simulative data and field data. For field data verification, the interharmonic content obtained by the proposed algorithm, the method explained in [23], and the standard FFT algorithm are compared with the interharmonic content obtained from FFT when the FFT window length is adjusted to fit an integer multiple of the fundamental frequency as given in [29]. All algorithms of the proposed method are implemented using MATLAB running on Windows XP. The total computation time for a 1 min input data is almost 75 s. However, this computation time can be reduced much more by using a faster compiling environment such as C and a faster processor. The code can also be optimized for efficient computation.

3.2.1.1 Analysis on Simulative Data

Two different synthetic power signals with various interharmonic contents are considered in this part. The error between the correct first interharmonic value, both computed as group interharmonic and subgroup interharmonic according to the IEC standard [16], are compared with the results of the proposed approach, the method explained in [23] and the standard FFT approach with the window length of $200ms$. First interharmonics are considered, because the leakage effect due to the fundamental frequency deviation mainly affect the interharmonics around the fundamental frequency. The nominal value of the fundamental frequency is $50Hz$ and it is assumed to be varying from $49.8Hz$ to $50.2Hz$ since this has been observed in the field voltage data collected at the arc furnace plants [7, 10]. Extreme cases of $49.5Hz$ and $50.5Hz$ are also considered in the simulative analysis. In the IEC standard [16], for $50Hz$ power system, group interharmonic computation is given as

$$C_{ig,n}^2 = \sum_{i=1}^{9} C_{k+i}^2, \tag{3.25}$$

and the subgroup interharmonic computation is given as

$$C_{isg,n}^2 = \sum_{i=2}^{8} C_{k+i}^2, \tag{3.26}$$

where k represents the spectral component index for $5Hz$ resolution (i.e. $k = 10$ for the fundamental of $50Hz$), n is the harmonic number (i.e. $n = 1$ for the fundamental), C_{k+i} is the rms value of the $(k+i)^{th}$ spectral component, and $C_{ig,n}$ and $C_{isg,n}$ are the rms values of the interharmonic centered group and subgroup of order n, respectively (for example, the subgroup between $n = 5$ and $n = 6$ is designated as $C_{isg,5}$). The tests in this part are achieved for $n = 1$ case.

Case-1: Single interharmonic case

The time window of $200ms$ results in $5Hz$ frequency resolution for DFT components. Therefore, to obtain the interharmonic frequencies around the fundamental frequency using Kalman filtering, twenty-state Kalman filter model is used (from $f = 0$ to $45Hz$ with $5Hz$ resolution both for in-phase and quadrature-phase components). In this case the signal $x(t) = sin(2\pi ft) + 0.5sin(2\pi 65t)$ is considered with the fundamental frequency f. If no leakage effect existed, i.e. $f = 50.00Hz$, the interharmonic subgroup-1 (interharmonics between the fundamental frequency and the 2^{nd} harmonic) and the interharmonic group-1 would both be equal to 0.50 when the FFT algorithm is applied, since the amplitude of the only interharmonic frequency is 0.50. Otherwise, when the fundamental frequency is not exactly $50Hz$, leakage effect is observed. Subgroup and group interharmonic computations are achieved according to [16]. The results are given in Table 3.1. It is observed in Table 3.1 that the method in [23] has no error for both group and subgroup interharmonic computations, which is due to the fact that this method provides the exact interharmonic content of the signal when the fundamental frequency is determined precisely. With the classical FFT approach with a standard window of $200ms$ long, the error in the first subgroup interharmonic value may reach 3.12%, when the frequency deviates between $49.8Hz$ and $50.2Hz$, which was the case observed in the field data collected at the HV transformers supplying the arc furnace plants [10]. For the extreme case of $49.5Hz$, standard FFT results in an error of 7.76% and 9.40% for subgroup and group first interharmonics, respectively. Finally for the Kalman

Table 3.1: Both group and subgroup interharmonic-1 computed with the standard FFT computation (FFT), the method in [23] and the proposed method (PM) for $x(t) = sin(2\pi ft) + 0.5sin(2\pi 65t)$

$f(Hz)$	Interharmonic-1 subgroup						Interharmonic-1 group					
	FFT	error (%)	Mtd in [23]	error (%)	PM	error (%)	FFT	error (%)	Mtd in [23]	error (%)	PM	error (%)
49.50	0.54	7.76	0.50	0.00	0.4966	0.68	0.55	9.40	0.50	0.00	0.4980	0.40
49.80	0.52	3.12	0.50	0.00	0.4974	0.52	0.52	3.44	0.50	0.00	0.4983	0.34
49.90	0.51	1.54	0.50	0.00	0.4976	0.48	0.51	1.62	0.50	0.00	0.4984	0.32
49.95	0.51	0.76	0.50	0.00	0.4978	0.44	0.50	0.78	0.50	0.00	0.4985	0.30
50.00	0.50	0.00	0.50	0.00	0.4979	0.42	0.50	0.00	0.50	0.00	0.4986	0.28
50.05	0.49	0.74	0.50	0.00	0.4979	0.42	0.48	0.72	0.50	0.00	0.4986	0.28
50.10	0.49	1.46	0.50	0.00	0.4979	0.42	0.49	1.38	0.50	0.00	0.4986	0.28
50.20	0.48	2.84	0.50	0.00	0.4977	0.46	0.49	2.44	0.50	0.00	0.4985	0.30
50.50	0.47	6.10	0.50	0.00	0.4963	0.74	0.48	3.40	0.50	0.00	0.4977	0.46

filtering based method, the error value is around 0.45% and 0.30% for subgroup and group interharmonic computations respectively as given in Table 3.1, which shows the Kalman filtering based method is successful in estimating the interharmonics without applying two FFT algorithms and precise fundamental frequency detection as in the case of [23]. The maximum errors are observed for $f = 50.5Hz$ and they are 0.74% and 0.46% for the first subgroup and group interharmonics, respectively, as shown in Table 3.1. Only the first two decimal digits are shown in all tables for the sake of simplicity.

Case-2: Interharmonics at various frequencies case

In this case the signal $x(t) = sin(2\pi ft) + 0.7sin(2\pi 53t) + 0.6sin(2\pi 55t) + 0.5sin(2\pi 58t) + 0.4sin(2\pi 62t) + 0.3sin(2\pi 65t)$ is considered with the fundamental frequency f. If no leakage effect existed, the interharmonic subgroup-1 would be equal to 0.62 and the interharmonic group-1 would be 0.96 (these are computed for the case of $f = 50.00Hz$). The aim of this case is to test the proposed method with a signal similar to the field data. There are various interharmonics between the fundamental and the second harmonics with decreasing amplitudes from the fundamental frequency towards the second harmonic.

Table 3.2: Both group and subgroup interharmonic-1 computed with the standard FFT computation (FFT), the method in [23] and the proposed method (PM) for $x(t) = sin(2\pi ft) + 0.7sin(2\pi 53t) + 0.6sin(2\pi 55t) + 0.5sin(2\pi 58t) + 0.4sin(2\pi 62t) + 0.3sin(2\pi 65t)$

$f(Hz)$	Interharmonic-1 subgroup						Interharmonic-1 group					
	FFT	error (%)	Mtd in [23]	error (%)	PM	error (%)	FFT	error (%)	Mtd in [23]	error (%)	PM	error (%)
49.50	0.68	9.01	0.62	0.00	0.5682	4.12	1.07	11.59	0.96	0.00	0.9271	3.92
49.80	0.64	3.28	0.62	0.00	0.6948	0.96	1.01	4.55	0.96	0.00	0.9450	3.29
49.90	0.63	1.54	0.62	0.00	0.6052	0.61	0.99	2.26	0.96	0.00	0.9504	3.20
49.95	0.63	0.76	0.62	0.00	0.6107	0.54	0.98	1.68	0.96	0.00	0.9532	1.45
50.00	0.62	0.00	0.62	0.00	0.6163	0.33	0.96	0.00	0.96	0.00	0.9558	2.98
50.05	0.62	0.71	0.62	0.00	0.6219	0.56	0.95	1.11	0.96	0.00	0.9582	3.00
50.10	0.61	1.37	0.62	0.00	0.6276	0.74	0.94	2.19	0.96	0.00	0.9603	3.03
50.20	0.61	2.47	0.62	0.00	0.6387	1.66	0.92	4.25	0.96	0.00	0.9633	3.09
50.50	0.60	4.08	0.62	0.00	0.6637	4.00	0.88	9.21	0.96	0.00	0.9575	3.14

It is observed in Table 3.2 that the proposed method is again successful in computing the first interharmonic value. The maximum error observed in the fundamental frequency range of $49.5Hz$ and $50.5Hz$ is 4.12% and 3.92% for subgroup and group first interharmonics, respectively, as shown in Table 3.2.

3.2.1.2 Analysis on Field Data

Field data are collected at an arc furnace plant at the MV side. Sampling rate is $3.2kHz$ (i.e. $640 samples/10 cycles$ for the ideal case of $f = 50Hz$) as in the case in [23]. The proposed algorithm is applied to the voltage waveform collected during the boring phase of the arc furnace operation, where the frequency deviates significantly. The rms voltage and the corresponding frequency at one phase is shown in Figure 3.5. The corresponding frequency of one phase is computed using Kalman filtering. The fundamental frequency is determined as the state variable of the EKF and the fundamental frequency deviation is obtained at the output of the EKF. During this test process, the same approach given in [23] is followed. The voltage is normalized to have unity amplitude at the $50Hz$ component to make the results comparable with the analysis on simulative data case.

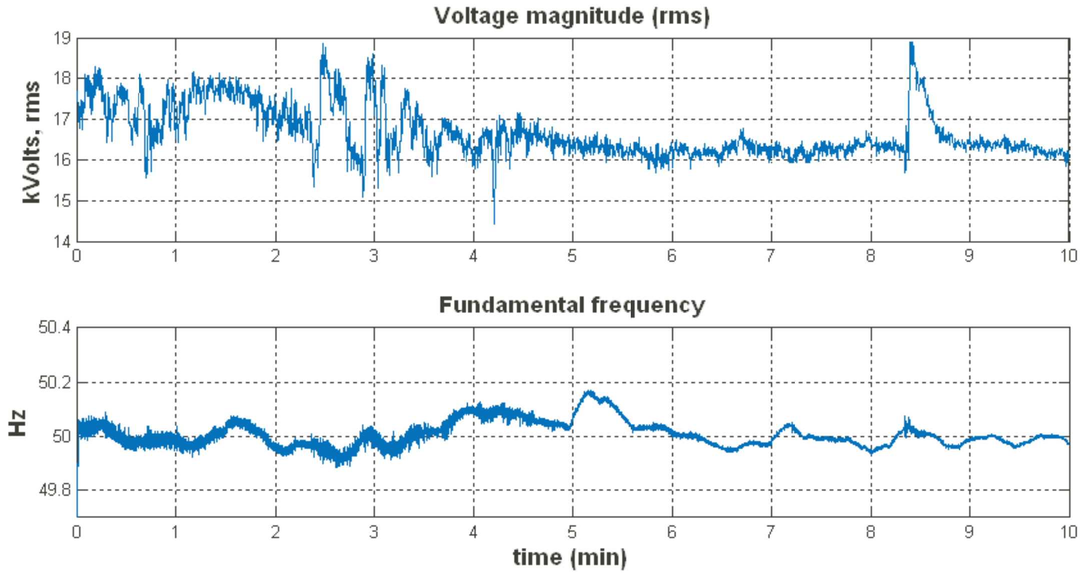

Figure 3.5: Magnitude and the fundamental frequency variation of the field data collected at the MV side of the power system supplying an arc furnace plant. Fundamental frequency deviation is obtained by using EKF.

To form a reference for the interharmonic computation, resampling through interpolation is achieved on the 10-cycle windows of the waveform as proposed in [29]. The data is resampled such that 640 samples exactly match the 10-cycle of the waveform. This changes the frequency resolution slightly, but the leakage due to spreading of the fundamental frequency does not exist any more; however, as mentioned in [23], it is important to note that the interpolation process may distort the frequency content of the signal. But it is still much closer to the exact solution than the standard FFT is, therefore it is used here for comparison purposes. Interharmonic-1 is computed with group method of the IEC standard [16]. The interharmonics computed with the proposed method, the method in [23] and the standard FFT computation of $200ms$ windows are compared with the reference interharmonics. The results are given in Table 3.3. It is observed that the proposed method gives better results than the standard FFT algorithm, computes interharmonics much closer to the reference values computed using the algorithm given in [29]. Although for some frequencies, the proposed method results are worse than the results of the method in [23], the proposed method has some advantages over the method in [23]. In the proposed method, since FFT algorithm is not applied for interharmonic analysis, there is no leakage effect

Table 3.3: Group computation of interharmonic-1 with the proposed method, the method in [23], the standard FFT computation (FFT) and the FFT+interpolation method on field data. Error values are computed assuming that the FFT+interpolation gives reference results.

	Group Interharmonic-1						
Fundamental Freq (Hz)	FFT+Interpolation (Reference)	Proposed Method	error (%)	Method in [23]	error (%)	Standard FFT	error (%)
49.90	0.163	0.162	**0.85**	0.162	0.61	0.178	8.94
49.93	0.160	0.160	**0.25**	0.149	6.83	0.236	47.50
50.02	0.131	0.135	**3.21**	0.129	1.51	0.148	12.98
50.12	0.162	0.167	**2.79**	0.165	2.96	0.188	12.58
50.15	0.165	0.168	**2.06**	0.166	0.60	0.175	6.06

problem. This also reduces the computational complexity. Furthermore, there is no need for precise detection of the fundamental frequency, which means that fundamental frequency deviation is not so critical in the proposed method. The percentage difference between the reference and the proposed method results are given in boldface in the Table 3.3.

3.2.2 Discussion

In this section of the thesis, a Kalman filtering based method for interharmonic computation is proposed for especially highly fluctuating fundamental frequency cases in the power system. Up to now, researches have shown that the system frequency deviates significantly due to the fluctuating current demands of some loads and disturbances or subsequent system transients in the power systems especially when an interconnected system does not exist. If a standard window length is used for the entire FFT analysis process, spectral leakage will occur and even non-existing interharmonics in the signal content will appear at the FFT output when the fundamental frequency deviates from the nominal value [23]. The proposed method uses Kalman filtering to obtain the spectral decomposition of the voltage waveform, which has some advantages over the FFT based spectral decomposition methods. Since FFT algorithm is not applied, the fundamental frequency deviation is not so critical, therefore no zero cross detection algorithm is applied in this method. Only by determining the fundamental frequency as a state variable of the EKF, which is the first Kalman filter in the method, the fundamental frequency is computed. Also in [23], to obtain the interharmonics, two FFT algorithms are applied which causes leakage effect problems in case of fundamental frequency deviation. However in the proposed method, for a certain frequency resolution, suitable state variables are determined for the Kalman filters and interharmonics of the waveform are obtained. Higher frequency resolution can be preferred for more precise estimates, although an increase in the frequency resolution has a cost of increasing the matrix dimensions of the state equations.

The proposed method consists of two Kalman filters, which are an EKF and a LKF. Initially an EKF is used which contains three state variables. These state variables are in-phase component of waveform (x_1), quadrature-phase component of the waveform (x_2) and finally fundamental frequency (x_3). The output of this filter gives the fundamental frequency and envelope of the voltage waveform as shown in Figure 3.3. In the second part of the proposed method, a twenty-state LKF is used. The DC component of the envelope of the waveform can be considered as a sinusoidal at $0Hz$. Therefore, for $5Hz$ frequency resolution case, to obtain the subgroup and group computation of interharmonic-1, which are the interharmonics between the fundamental and the second harmonic, the voltage envelope is defined as the sum of ten sinusoidals at the corresponding frequencies of $0, 5, 10, 15, 20, \cdots, 45Hz$. Since for each of these sinusoidals, two state variables of in-phase and quadrature-phase components are determined, a twenty-state LKF model is obtained and the output of this LKF gives the spectral amplitudes at the corresponding frequencies. In fact, to obtain the spectral decomposition of the waveform, only a single Kalman filter can be used. In the proposed method, the fundamental frequency is computed by the EKF. If it is not necessary to obtain the fundamental frequency, only by using one LKF, the spectral decomposition around the fundamental can be obtained. For this case, a 38-state LKF model is used to obtain the interharmonics around the fundamental. Equation (3.8) can be rewritten as given in

$$v(t) = Vcos(2\pi ft) + \sum_{i=1}^{N} \frac{\Delta V_i}{4} \left\{ cos(2\pi(f + f_{fi})t + \phi_i) + cos(2\pi(f - f_{fi})t + \phi_i) \right\}. \tag{3.27}$$

As it is clearly observed from this equation that the effect of the modulation appear as interharmonics at beat frequencies which are $f \mp f_{fi}$ in the spectrum. For $5Hz$ frequency resolution case, to obtain the interharmonics around the fundamental, voltage waveform, $v(t)$, can be considered as the sum of nineteen sinusoidal waveforms at frequencies $5, 10, 15, \cdots, 90, 95Hz$. For each of these waveforms, two state variables of in-phase and quadrature-phase components are determined and a 38-state LKF model is obtained. The output of the LKF gives the spectral amplitudes at the interharmonics around the fundamental, directly. Although the matrix dimensions of the state equations are increased, the advantage of this approach is that in stead of using two types of Kalman filters, only a single LKF is enough to obtain the same result.

This method provides good estimates of the interharmonics at frequencies around the fundamental frequency. Since interharmonics are the main cause of flicker, the method can also be used for flicker estimation algorithms, which are based on spectral decomposition (such as [7] and [5]). In Section 3.3, such kind of a flicker estimation algorithm which is based on Kalman filtering is explained.

In this method, the window length is selected as $200ms$ as recommended in the IEC Standard [16]. Therefore, for applications other than power quality, such as real-time control and protection applications, which require response times of the order of a couple of cycles, the method can be modified to use sliding windows of $200ms$ overlapping one or two cycles, to be able to get updated values every one or two cycles.

3.3 Flicker Evaluation Based on Kalman Filtering

Spectral decomposition obtained with Kalman filters is explained in detail in the previous Section 3.2. In the proposed algorithm, $\Delta V_i/V$ values corresponding to the flicker frequencies are obtained by applying an EKF and a LKF consecutively on voltage waveform using 10 cycle time windows which corresponds to window length of $200ms$ for the $50Hz$ power system. Since Kalman filters are used to estimate the signal spectrum, no leakage problem occurs, which is an important advantage and novelty of this method.

Interharmonics are known to be the main cause of flicker; therefore, the spectral decomposition obtained by Kalman filtering, which is explained in Section 3.2, is used here as a part of the proposed flicker estimation algorithm. The flicker estimation approach in Chapter 2 is used; however, this time, the spectral decomposition is obtained by Kalman filtering, not by applying FFT algorithm. The block diagram of the proposed light flicker estimation method, which is also explained in [19], is given in Figure 3.6. In this diagram, the sampled input signal is denoted by $v(t)$. Initially, in order to get rid of the harmonic effect, a low pass filter (LPF) with a corner frequency at $75Hz$ is applied. Then for each time window of ten cycles, the spectral decomposition is obtained by applying two Kalman filters, EKF and LKF, consecutively. The EKF and LKF algorithms are implemented based on [27].

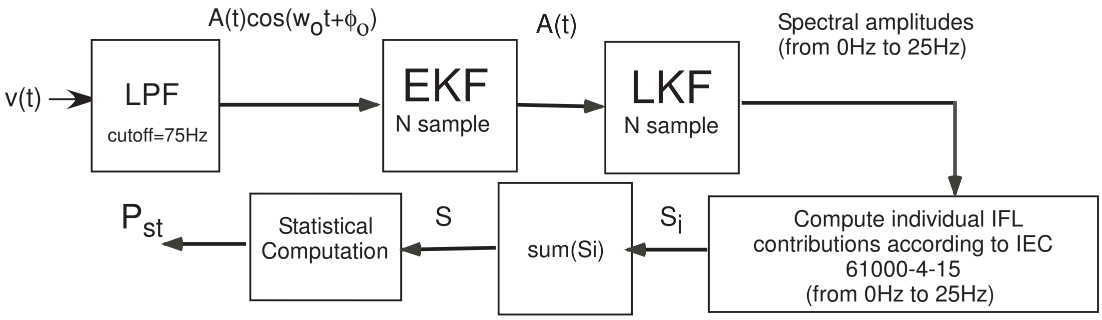

Figure 3.6: Block diagram of the proposed flicker estimation method.

Since the voltage signal in EAF plants contains different flicker frequencies, the voltage fluctuation is modeled as given in (2.2), which is again pointed out here as,

$$v(t) = cos(2\pi f t + \phi_o)) \left\{ V + \sum_{i=1}^{N} \frac{\Delta V_i}{2} cos(2\pi f_{fi} t + \phi_i) \right\}. \tag{3.28}$$

The signal model in (3.28) can also be modeled as a sinusoidal voltage waveform with time varying amplitude A(t), where $A(t) = V + \sum_{i=1}^{N} \frac{\Delta V_i}{2} cos(2\pi f_{fi} t + \phi_i)$.

This signal model is shown as

$$\begin{aligned} v(t) &= \{cos(2\pi ft + \phi_o)\}\, A(t), \\ &= cos(\phi_o)cos(2\pi ft)A(t) - sin(\phi_o)sin(2\pi ft)A(t). \end{aligned} \tag{3.29}$$

In (3.29), $A(t)$ represents the time varying amplitude of the input signal. In order to obtain the spectral decomposition for the consecutive windows, EKF is applied on the voltage waveform to obtain the envelope, $A(t)$. The procedure of obtaining the voltage envelope, $A(t)$, by applying EKF is explained in Section 3.2 in detail. The state variables for this EKF algorithm are determined as, in-phase component of v(t) (x_1), quadrature-phase component of v(t) (x_2), and finally fundamental frequency of v(t) (x_3).

Fundamental frequency deviation is frequently observed in EAF field data [7, 19]. Since fundamental frequency is not a constant in the EKF algorithm, it is also determined as the state variable, x_3. Consequently, fundamental frequency of the voltage waveform is also estimated successfully with the proposed spectral decomposition method as explained in Section 3.2. Therefore, there is no extra fundamental frequency computation algorithm in contrast to the FFT based method given in Chapter 2, which is also proposed in [7]. The voltage signal is a nonlinear function of the state variable, x_3, therefore the state transition and measurement equations are nonlinear functions of x_3. In EKF algorithm state transition and measurement equations are combined together in accordance with the EKF model explained in [28] and the EKF model is realized. By applying EKF on the voltage waveform, its envelope, $A(t)$, is obtained. The linearized state transition matrix, Φ, and the linearized measurement vector, H, for the EKF are given in Section 3.2 to explain the proposed spectral decomposition method. The EKF algorithm is formed by using the linearized state transition matrix, Φ, and the linearized measurement vector, H. Then using the estimated state variables of the state vector, which is the output of the EKF algorithm, the envelope of the voltage waveform and the fundamental frequency variation are obtained. The envelope of the voltage waveform is formed by using the state variables x_1 and x_2 as

$$A(t) = \sqrt{\hat{x}_1(t)^2 + \hat{x}_2(t)^2}. \tag{3.30}$$

The variation of the state variable x_3 gives the time-varying fundamental frequency, which is represented as

$$f(t) = \hat{x}_3(t). \tag{3.31}$$

Then, using a second Kalman filter model, which is LKF, spectral decomposition of the voltage waveform is obtained. The input of the LKF is the envelope of the voltage waveform, $A(t)$, which is the output of EKF and contains different flicker frequency components. The mathematical representation of the envelope of the voltage waveform, $A(t)$, is

$$A(t) = \left\{ V + \sum_{i=1}^{N} \frac{\Delta V_i}{2} cos(2\pi f_{fi} t + \phi_i) \right\}. \tag{3.32}$$

The envelope of the voltage waveform, $A(t)$, is the measurement of the LKF algorithm as given in the spectral decomposition method in Section 3.2. In the FFT based method given in Chapter 2 [7], S is evaluated by using the frequency spectrum of signal $v(t)$ from $f - 25Hz$ to $f + 25Hz$ where f is the fundamental frequency and $25Hz$ is the maximum flicker frequency given in Table 2.1. However, in the Kalman filtering based method, the output of the EKF algorithm is the envelope of the voltage fluctuation, $A(t)$, directly. Therefore, spectral decomposition of $A(t)$ is obtained by using a LKF for flicker frequencies, f_{fi}, in the $0 - 25Hz$ frequency region. In equation (3.32), since V is constant, it can be considered as a DC voltage signal. In the proposed method, $A(t)$ is represented as the summation of six sinusoidal voltage fluctuations at frequencies $0, 5, 10, 15, 20, 25Hz$. $5Hz$ resolution is selected so that the results can be compared with $5Hz$ resolution results of the proposed method in Chapter 2. Higher frequency resolution can be preferred for more precise estimates, although frequency resolution increase has a cost of increasing the matrix dimensions of the state equations. For one of these sinusoidal voltage fluctuations, the in-phase and the quadrature-phase components, which are determined as the two state variables for the corresponding voltage fluctuation in the LKF model, are obtained from sinusoidal expansion of the voltage fluctuation as

$$\frac{\Delta V_i}{2} cos(2\pi f_{fi} t + \phi_i) = \frac{\Delta V_i}{2} cos(\phi_i) cos(2\pi f_{fi} t) - \frac{\Delta V_i}{2} sin(\phi_i) sin(2\pi f_{fi} t). \tag{3.33}$$

In (3.33), states are defined as follows:
x_1 = in-phase component of the sinusoidal fluctuation ($\frac{\Delta V_i}{2} cos(\phi_i)$)
x_2 = quadrature-phase component of the sinusoidal fluctuation ($\frac{\Delta V_i}{2} sin(\phi_i)$)
$i = 1, 2, \cdots, 6$ represents the frequencies $0, 5, 10, 15, 20, 25Hz$

The LKF model which is developed to obtain the spectral components of the envelope of the signal, $A(t)$, which contains six sinusoidal voltage fluctuations at different flicker frequencies is given in equations (3.35) and (3.36).

Let's define the state vector of the LKF, $\bar{x}_k$, as

$$\bar{x}_k = \begin{bmatrix} x_{1,1} & x_{2,1} & x_{1,2} & x_{2,2} & \cdots & x_{1,6} & x_{2,6} \end{bmatrix}_k^T \tag{3.34}$$

where superscript T defines transpose of the vector given in brackets and

$x_{1,i}$ = in-phase component of the sinusoidal fluctuation at flicker frequency, f_{fi}
$x_{2,i}$ = quadrature-phase component of the sinusoidal fluctuation at flicker frequency, f_{fi} ($f_f = \{0, 5, 10, 15, 20, 25\}$)

Then the state transition equation for the twelve-state Kalman filter model is given as

$$\bar{x}_{k+1} = \begin{bmatrix} 1 & 0 & \cdots & 0 \\ 0 & 1 & \cdots & 0 \\ \vdots & \vdots & \ddots & \vdots \\ 0 & 0 & \cdots & 1 \end{bmatrix} \bar{x}_k + \bar{w}_k. \tag{3.35}$$

Since the state variables $x_{1,i}$ and $x_{2,i}$ represent the in-phase and quadrature-phase components of the f_{fi} voltage phasor, the measurement equation is formed as

$$z_k = \beta \bar{x}_k + v_k, \tag{3.36}$$

where the corresponding measurement vector, β, is

$$\beta = \begin{bmatrix} cos(2\pi f_{f1} t) & -sin(2\pi f_{f1} t) & cos(2\pi f_{f2} t) & -sin(2\pi f_{f2} t) & \cdots & cos(2\pi f_{f6} t) & -sin(2\pi f_{f6} t) \end{bmatrix} \tag{3.37}$$

In this twelve-state LKF model, which is formed by equations (3.35) and (3.36), $\bar{w}_k$ represents the process noise vector and v_k represents the measurement noise vector. The spectral amplitude at flicker frequency f_{fi} is obtained by using the corresponding state variables $x_{1,i}$ and $x_{2,i}$, which are calculated for each time window. The result $\sqrt{\hat{x}_{1,i}^2 + \hat{x}_{2,i}^2}$ gives the spectral amplitude at flicker frequency f_{fi} for the corresponding time window.

In the proposed method since the spectral amplitudes are obtained with $5Hz$ resolution, flicker frequencies in $0-25Hz$ frequency region, f_{fi}, are determined as $0, 5, 10, 15, 20$ and $25Hz$ and twelve-state LKF model is obtained. However, it is possible to obtain higher resolution for more accurate results, but this will increase the number of states.

The spectral decomposition is obtained from $0Hz$ to $25Hz$ with $5Hz$ resolution for each 10 cycle time window by applying EKF and LKF consecutively. The $\frac{\Delta V_i}{V}$ value in equation (3.1) is obtained from this spectrum and S_i is calculated as given in (3.1). Finally, the instantaneous flicker sensation, S, is obtained as the summation of all S_i.

3.4 Verification of the Proposed Method for Flicker Analysis

For verification of the proposed method, a digital realization of the IEC flickermeter given in [9] is used to compare the response of the method to the actual IEC flickermeter behavior with the proposed method. Both simulated and field data are used.

3.4.1 Verification with Simulated Data

Simulated data is produced by modulating the sine wave at $50Hz$ system frequency as given in (2.2) with various flicker frequencies and the corresponding $\Delta V/V$ values in Table 2.1 with a sampling frequency of $3200Hz$. The data length is 10 minutes. S is computed with the proposed method and the results are compared with the results of the digital realization of the IEC flickermeter.

Table 3.4: Proposed light flicker estimation algorithm response for sinusoidal voltage fluctuations

Input voltage fluctuation to obtain $S=1$ with IEC flickermeter		Proposed flickermeter response			
		$5Hz$ resolution		$0.5Hz$ resolution	
flicker freq.(Hz)	$\Delta V/V\%$	S	error(%)	S	error(%)
5.0	0.40	1.01	1.0	1.00	0.0
10.0	0.26	1.00	0.0	0.99	-1.0
12.0	0.31	0.99	-1.0	0.99	-1.0
15.0	0.43	0.98	-2.0	0.99	-1.0
20.0	0.70	0.99	-1.0	0.99	-1.0
25.0	1.04	1.02	2.00	1.02	2.0

3.4.1.1 Test 1: Single Flicker Frequency Case

The single sinusoidal flicker frequency case is given in (2.1). It is expected that S should be close to unity since Table 2.1 given in [1] is for unity S response to sinusoidal voltage fluctuations. The experiment is repeated with both $5Hz$ and $0.5Hz$ resolutions. The size of state vector is 6 in $5Hz$ resolution. However when we increase the resolution rate to $0.5Hz$, the size of state vector increases to 51 which means that resolution increase has a cost of increasing the number of state equations. In case of $0.5Hz$ resolution, summation of all S_i given in (3.1) from $0.5Hz$ to $25Hz$ with $0.5Hz$ increments are used to obtain S, whereas $\Delta V/V$ values corresponding to only $5, 10, 15, 20$ and $25Hz$ are added up to obtain S in case of $5Hz$ resolution. Comparison of the results with those of the IEC flickermeter are given in Table 3.4 for both resolution values.

3.4.1.2 Test 2: Combinations of Different Flicker Frequencies Case

In this test, the signal model in (3.28) is used to produce a voltage waveform at $3200Hz$ sampling frequency. The data length is again 10 minutes. This simulated voltage waveform is shown as

$$v(t) = \left\{ 1 + \frac{1}{2}\frac{10}{100} cos\left(\frac{2\pi 12t}{3200} + \frac{\pi}{6}\right) + \frac{1}{2}\frac{2}{100} cos\left(\frac{2\pi 5t}{3200} + \frac{\pi}{3}\right) \right\} cos\left(\frac{2\pi 50t}{3200}\right) \tag{3.38}$$

In Figure 3.7, simulated voltage waveform, $v(t)$, for one window length ($200ms$)

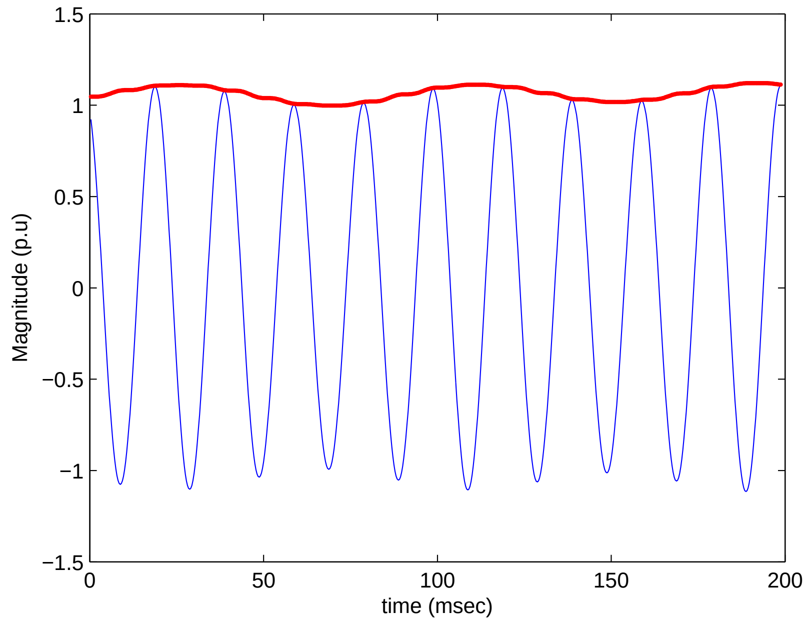

Figure 3.7: Simulated voltage waveform, $v(t)$, and the estimated envelope of $v(t)$ which is obtained by the EKF.

and the envelope of this voltage waveform, $A(t)$, which is estimated by the first stage (EKF algorithm) is shown. As it is shown in Figure 3.7, the envelope of the voltage waveform, $A(t)$, is obtained successfully with the EKF. The short term flicker severity, P_{st}, is equal to 22.53 with the proposed method, whereas it is equal to 24.18 with the digital implementation of the IEC flickermeter.

3.4.1.3 Test 3: Homogeneity of the Flickermeter Response

The Standard IEC-61000-4-15 requires that the flickermeter response should have the homogeneity property, i.e., whenever the $\Delta V/V$ value is doubled or halved, the resulting flicker severity P_{st} should also be doubled or halved respectively [1]. Homogeneity of the proposed algorithm is checked by applying twice and half of the $\Delta V/V$ values with the corresponding flicker frequencies given in Table 3.4. It is observed that the proposed method estimates P_{st} values with negligible error, always less than 1.5% as given in Table 3.5 which means that the homogeneity of the proposed algorithm holds. The error in this table is defined as the percentage difference between twice or half of the P_{st} computed

Table 3.5: Homogeneity of the proposed light flicker estimation algorithm

Flicker frequency (Hz) sinusoidal fluctuation	$\Delta V/V\%$ 230V/50Hz system	P_{st}	% Error
0.5	2.340	0.71	–
	2 × 2.340	1.41	+0.70
	0.5 × 2.340	0.36	-1.40
2.5	0.754	0.83	–
	2 × 0.754	1.66	0.00
	0.5 × 0.754	0.42	-1.20
5.0	0.398	0.69	–
	2 × 0.398	1.38	0.00
	0.5 × 0.398	0.35	-1.45
10.0	0.260	0.69	–
	2 × 0.260	1.38	0.00
	0.5 × 0.260	0.35	-1.45
12	0.312	0.70	–
	2 × 0.312	1.39	+0.71
	0.5 × 0.312	0.35	0.00
15	0.432	0.69	–
	2 × 0.432	1.37	+0.72
	0.5 × 0.432	0.35	-1.45
18	0.584	0.73	–
	2 × 0.584	1.46	0.00
	0.5 × 0.584	0.37	-1.37
20	0.700	0.69	–
	2 × 0.700	1.37	+0.72
	0.5 × 0.700	0.35	-1.45
25	1.042	0.70	–
	2 × 1.042	1.40	0.00
	0.5 × 1.042	0.35	0.00

and the P_{st} obtained by the proposed method when $\Delta V/V$ is doubled or halved.

3.4.2 Verification on AC Arc Furnace Data

Experiments on field data obtained at three different EAF plants are used to verify the effectiveness of the proposed algorithm in estimating the light flicker. The proposed light flicker estimation algorithm is used with $5Hz$ frequency resolution ($200ms$ windows). The data is obtained during the field measurements carried out through the National Power Quality Project of Turkey [22, 26]. EAF voltages are collected at a sampling rate of $3200Hz$ at the MV side of the EAF transformer [25]. Rms voltages collected at the MV side of the EAF transformers at those three plants are given with the instantaneous flicker sensation, S, values which is obtained from both the digital implementation of the IEC flickermeter and the proposed light flicker estimation algorithm in Figures 3.8, 3.9, and 3.10. In these figures, (a) shows the rms voltages with the P_{st} computed intervals, (b) shows the frequency variation, and (c) shows S computed by both the proposed method and the IEC flickermeter, for comparison purposes. The frequency variation is given to show that the proposed method gives good estimates irrespective of the frequency variation. It is observed that the proposed method gives good estimates of the instantaneous flicker sensation, S. More detailed views of S for the first two intervals for Figures 3.8, 3.9, and 3.10 are given in Figures 3.11, 3.12, and 3.13, respectively, for better comparison. To give a quantitative comparison of the algorithm, short term flicker severity, P_{st} is computed for the intervals given in the figures and the results are compared with both the results of the digital realization of the IEC flickermeter and the first proposed method which is also explained in [7] as given in Tables 3.6, 3.7 and 3.8. The results indicate good agreement between the IEC flickermeter and the proposed method which means that proposed method is successful in estimating the light flicker.

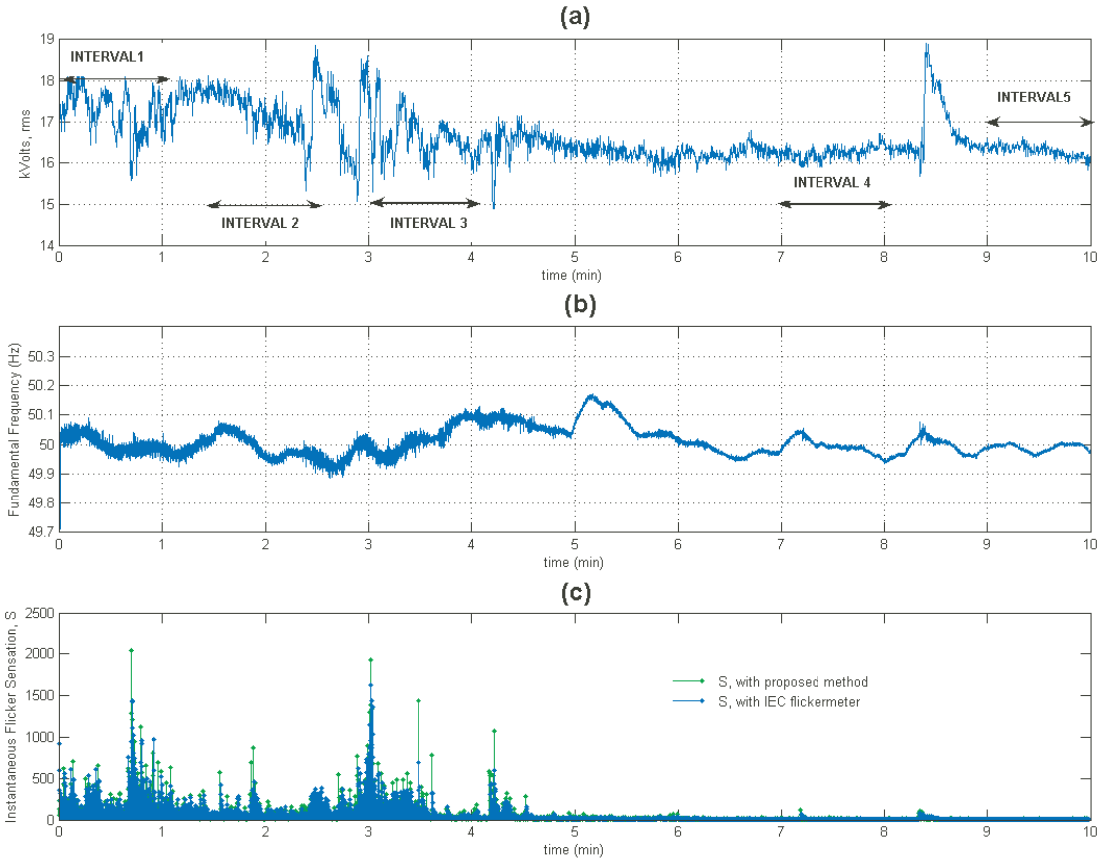

Figure 3.8: Plant-1 (a) rms voltage at the MV side of the EAF Plant with the P_{st} computed intervals, (b) fundamental frequency variation, (c) instantaneous flicker sensation, S.

Table 3.6: Short term flicker severity, P_{st}, computed inside the intervals given in Fig 3.8 with the proposed method, method in [7] and the digital realization of the IEC flickermeter

INTERVALS	IEC Flickermeter	Method in [7]	Err %	Proposed Mtd.	Err %
INTERVAL 1	15.4958	15.4131	+0.53	**15.5314**	**-0.23**
INTERVAL 2	9.5497	9.6166	-0.70	**9.5722**	**-0.24**
INTERVAL 3	13.2904	13.5436	-1.91	**13.2257**	**+0.49**
INTERVAL 4	2.6938	2.6922	+0.06	**2.7760**	**-3.05**
INTERVAL 5	1.8163	1.9905	-9.59	**1.9377**	**-6.68**

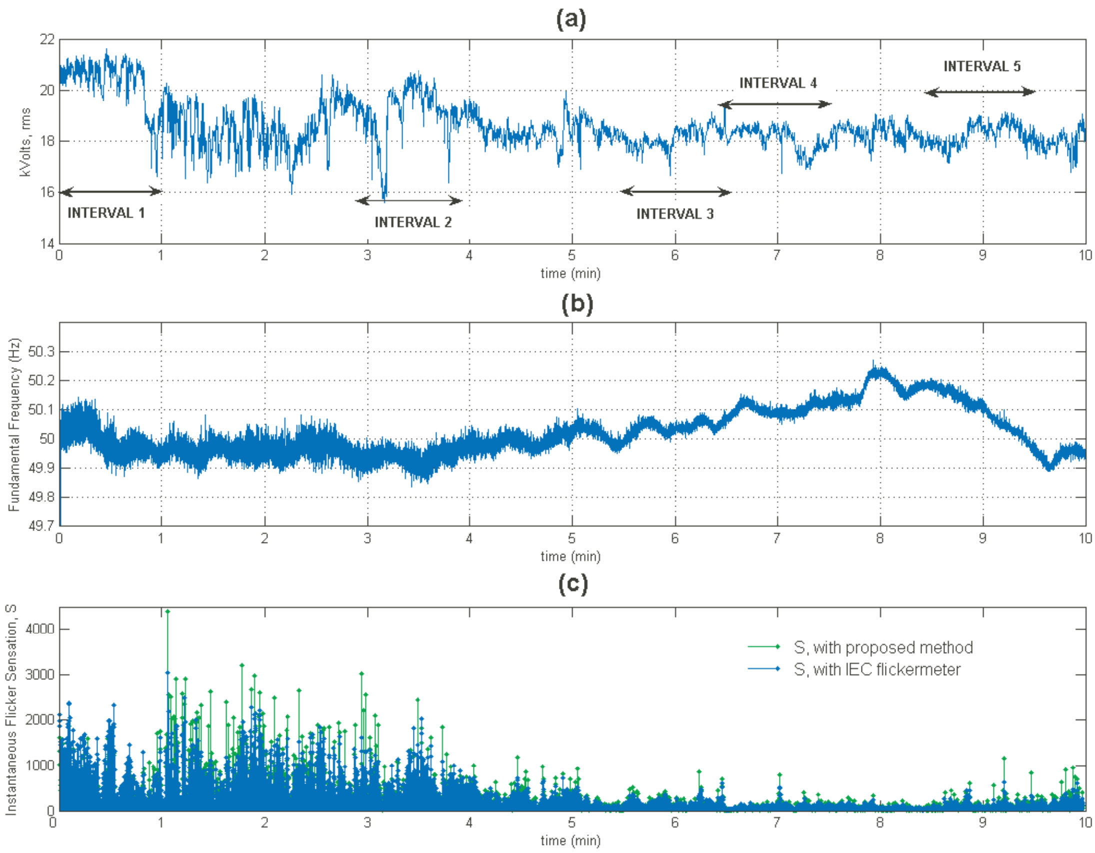

Figure 3.9: Plant-2 (a) rms voltage at the MV side of the EAF Plant with the P_{st} computed intervals, (b) fundamental frequency variation, (c) instantaneous flicker sensation, S.

Table 3.7: Short term flicker severity, P_{st}, computed inside the intervals given in Fig 3.9 with the proposed method, method in [7] and the digital realization of the IEC flickermeter

INTERVALS	IEC Flickermeter	Method in [7]	Err %	Proposed Mtd.	Err %
INTERVAL 1	22.3209	23.3268	-4.51	**22.0043**	**+1.42**
INTERVAL 2	21.4275	22.5856	-5.40	**22.1809**	**-3.52**
INTERVAL 3	11.5852	11.9070	-2.78	**11.6648**	**-0.69**
INTERVAL 4	9.2761	9.4001	-1.34	**9.0635**	**+2.29**
INTERVAL 5	10.6356	10.9129	-2.61	**10.8473**	**-1.99**

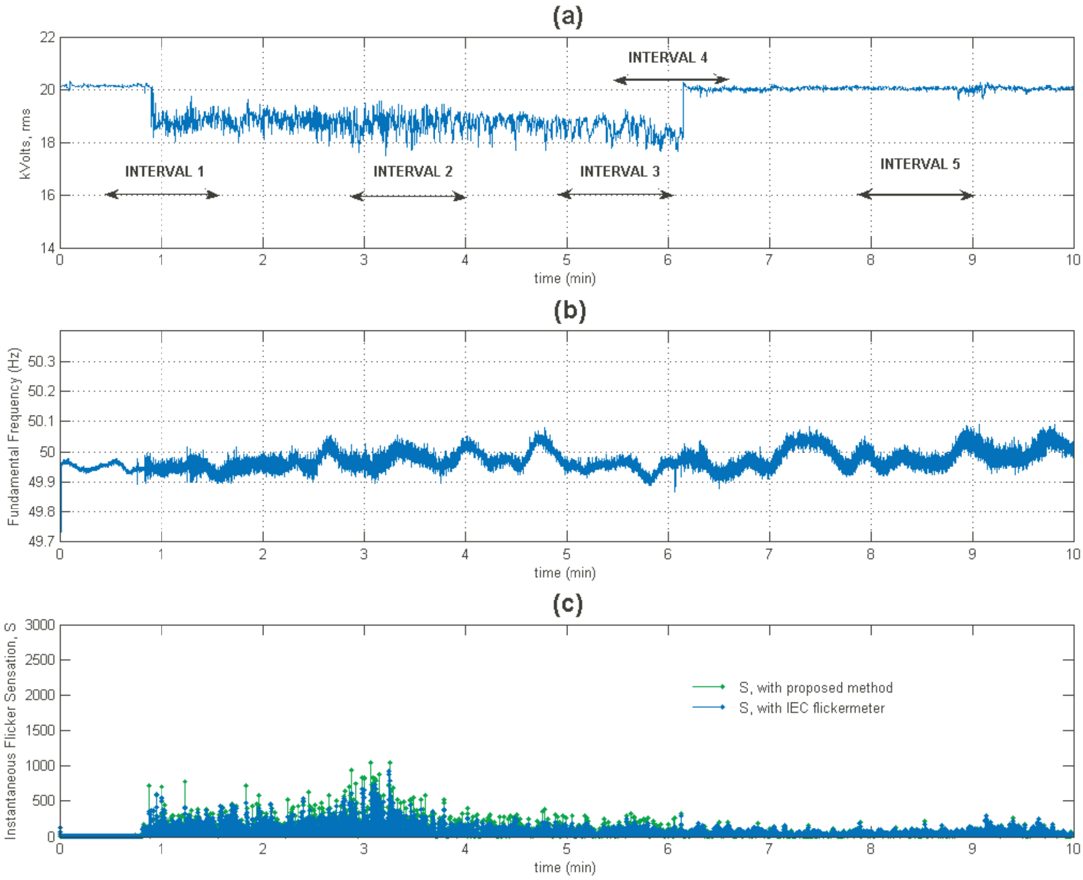

Figure 3.10: Plant-3 (a) rms voltage at the MV side of the EAF Plant with the P_{st} computed intervals, (b) fundamental frequency variation, (c) instantaneous flicker sensation, S.

Table 3.8: Short term flicker severity, P_{st}, computed inside the intervals given in Fig 3.10 with the proposed method, method in [7] and the digital realization of the IEC flickermeter

INTERVALS	IEC Flickermeter	Method in [7]	Err %	Proposed Mtd.	Err %
INTERVAL 1	11.6423	11.7285	-0.74	**11.9820**	**-2.92**
INTERVAL 2	16.0384	15.6946	+2.14	**15.9033**	**+0.84**
INTERVAL 3	9.0006	9.2464	-2.73	**9.1137**	**-1.26**
INTERVAL 4	8.2767	8.8416	-6.83	**8.7478**	**-5.69**
INTERVAL 5	6.4816	7.4208	-14.49	**5.9577**	**+8.08**

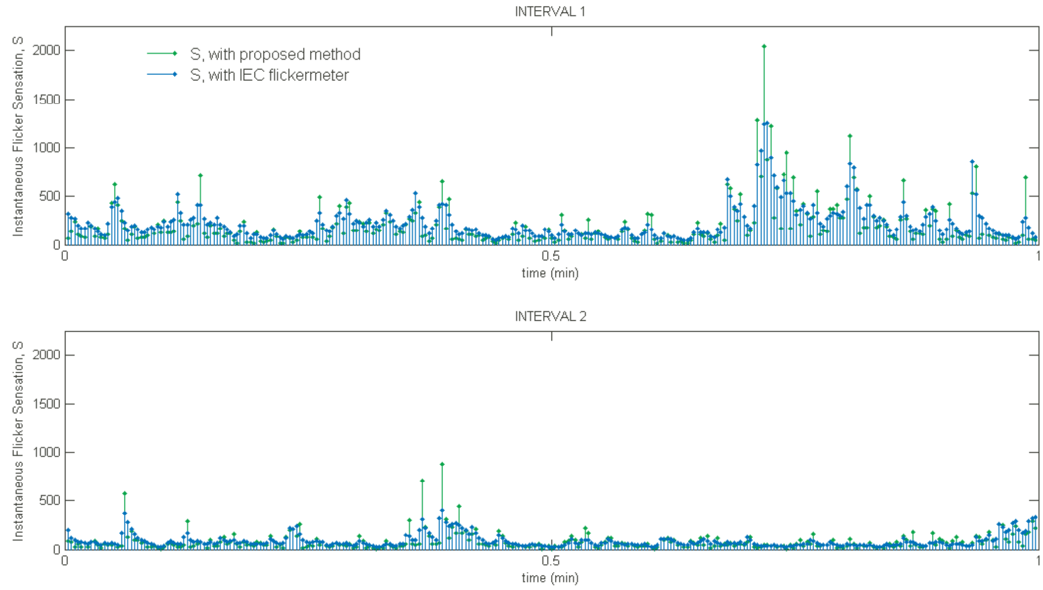

Figure 3.11: Plant-1 instantaneous flicker sensation, S, for Interval-1 and Interval-2 in Figure 3.8 for a more detailed comparison of the proposed method and the IEC flickermeter.

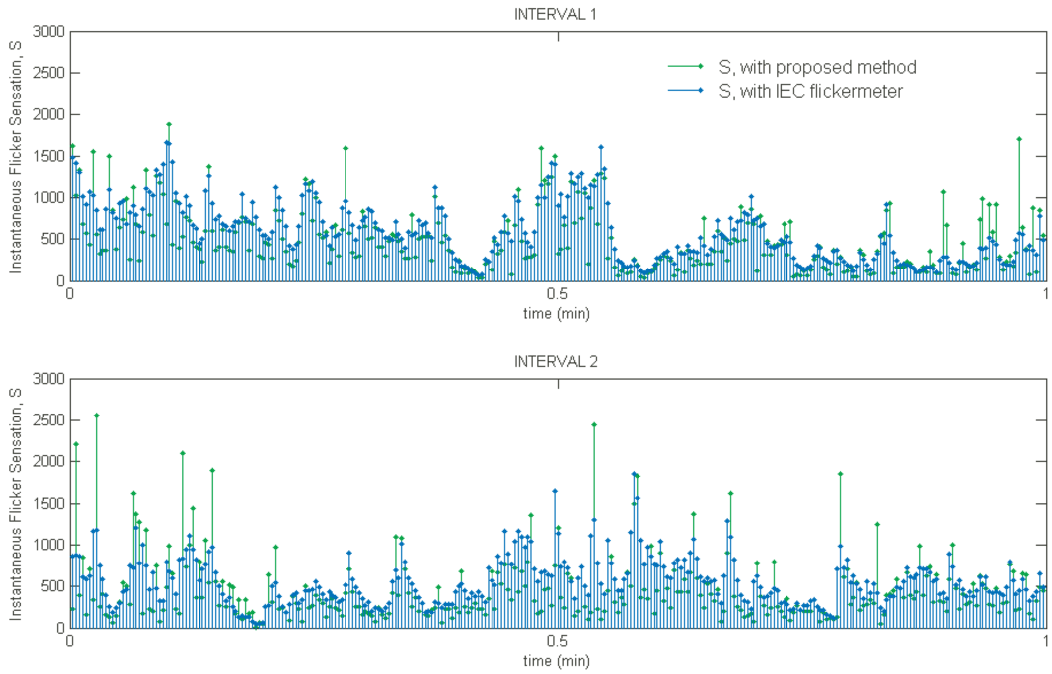

Figure 3.12: Plant-2 instantaneous flicker sensation, S, for Interval-1 and Interval-2 in Figure 3.9 for a more detailed comparison of the proposed method and the IEC flickermeter.

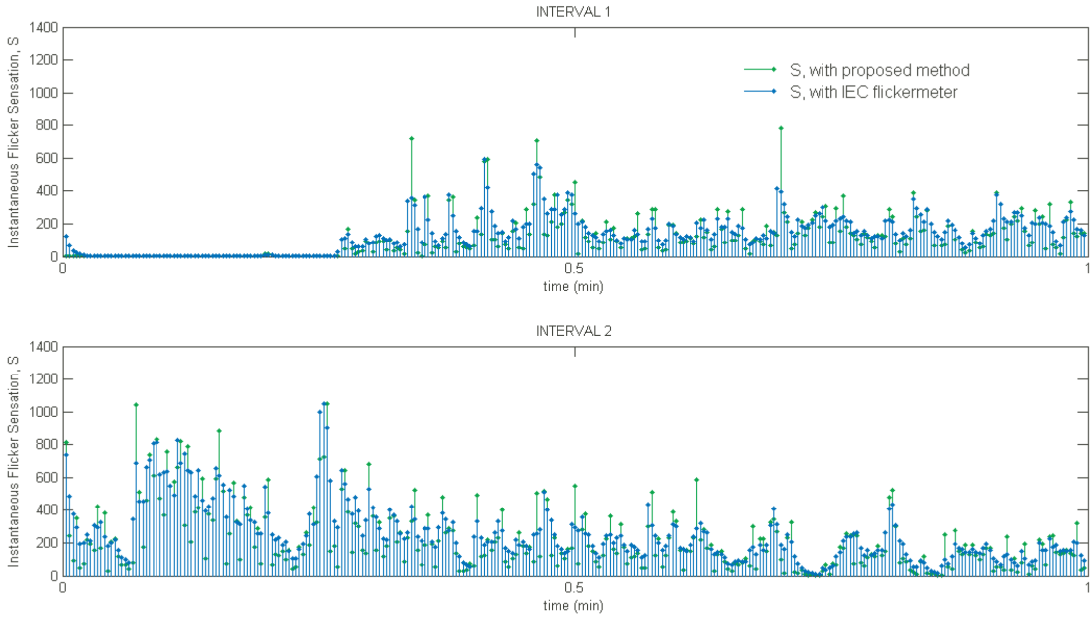

Figure 3.13: Plant-3 instantaneous flicker sensation, S, for Interval-1 and Interval-2 in Figure 3.10 for a more detailed comparison of the proposed method and the IEC flickermeter.

The calculation procedures are analyzed on a personal computer (PentiumIV, 2.20GHz). All algorithms are implemented using MATLAB running on Windows XP. The total computation time for a 1min input data is 75s. However, as mentioned in the spectral decomposition method part in Section 3.2, this computation time can be reduced much more by using a faster compiling environment such as C and a faster processor. The code can also be optimized for efficient computation.

The accuracy obtained on field data are comparable with the results given in [5] and in [2]. The mean error is 2.14%, 1.98%, and 3.76% for Plant-1, Plant-2 and Plant-3, respectively. In [2] mean error is around 6%. It varies between 0.44% and 5.94% in [5]. In [7] the mean error varies between 2.56% and 5.39% for different EAF plants.

Fundamental frequency for the three EAF plants are calculated by using EKF. Data length of each arc furnace data is chosen as 10 minutes and for each of them, histogram of the computed fundamental frequencies are obtained. The histogram of fundamental frequencies for Plant-1, Plant-2, and Plant-3 are shown in Figures 3.14, 3.15, and 3.16, respectively.

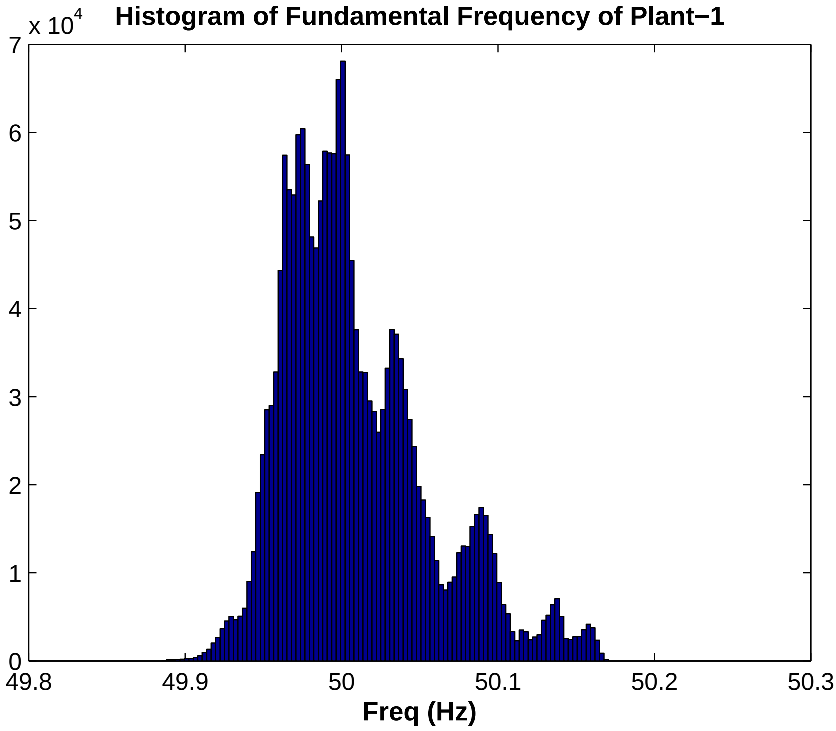

Figure 3.14: Histogram of fundamental frequency of Plant-1.

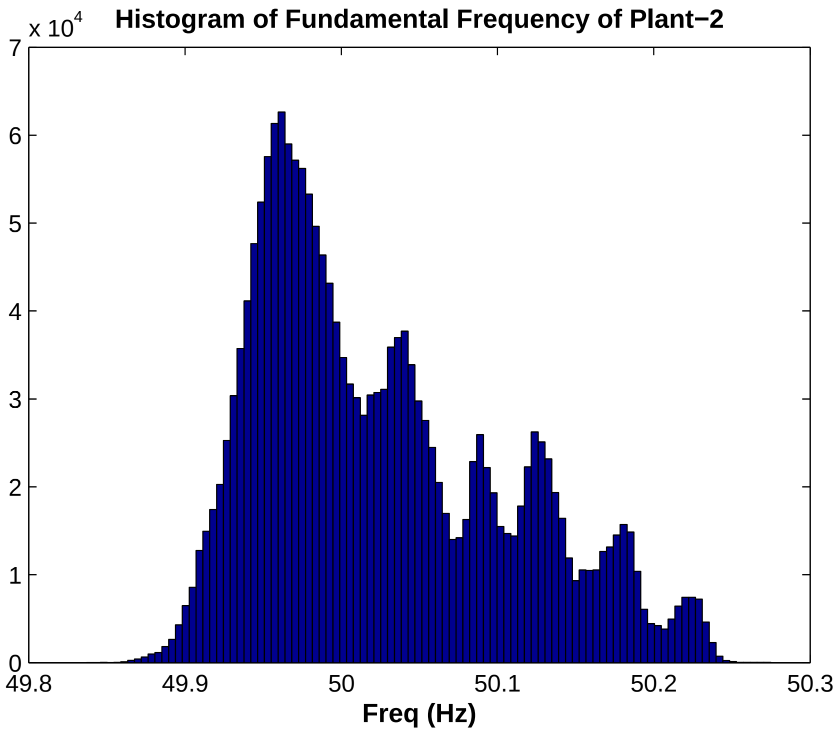

Figure 3.15: Histogram of fundamental frequency of Plant-2.

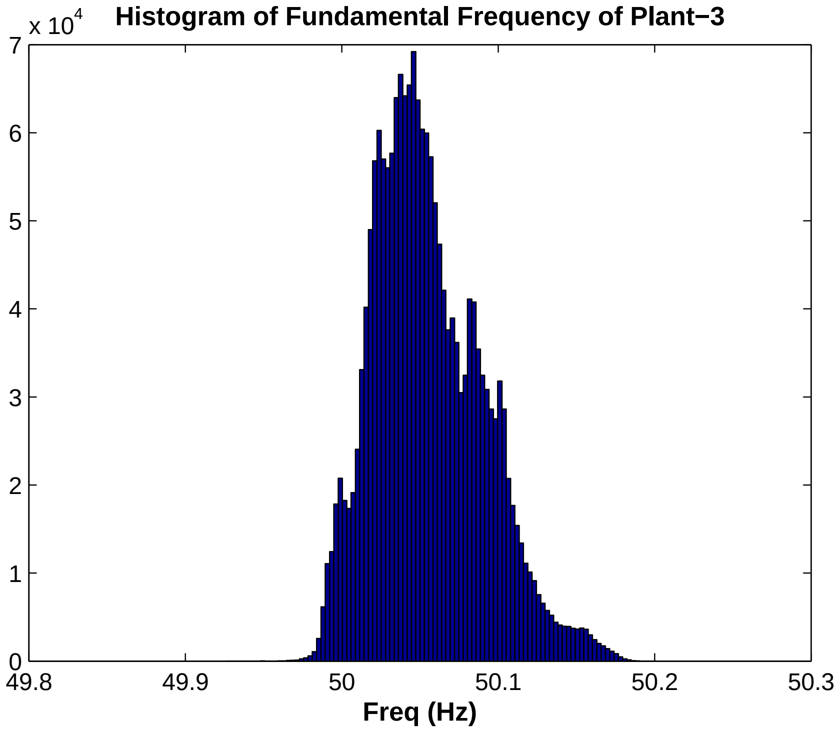

Figure 3.16: Histogram of fundamental frequency of Plant-3.

Since the histogram of fundamental frequency of each field data is similar to a Gaussian distribution form, we can again say that Kalman application provides quite satisfactory results.

CHAPTER 4

CONCLUSIONS

In this thesis, new flickermeter applications are proposed as alternatives to the IEC-flickermeter. Two different novel spectral-decomposition-based methods are proposed to estimate the light flicker of EAF plants, where the system frequency deviates significantly. The frequency deviation of the EAF plants is inside the range from $49.7Hz$ to $50.3Hz$, where the nominal system frequency is $50Hz$. In the first proposed method, spectral decomposition is obtained by utilizing the DFT algorithm on the voltage waveform directly using 10-cycle time windows. In the second method, spectral decomposition is obtained by utilizing two types of Kalman filters (EKF and LKF) consecutively. Again 10-cycle time windows are used, which coincides with the IEC harmonic and interharmonic computation standard [16].

For both of the proposed methods, instantaneous flicker sensitivity is obtained from the addition of contribution of each flicker-creating spectral component in the $25Hz$ neighborhood of the fundamental frequency. In the first method, leakage effect of the DFT algorithm in the case of deviated fundamental frequency is corrected by vector subtraction of the leakage DFT components from the DFT components of the original voltage waveform and the corrected spectral components are obtained. The leakage components are obtained from a pure sinusoidal waveform synthesized at the exact fundamental frequency. However, in the second method, the EKF algorithm computes the envelope of the voltage waveform and the fundamental frequency is eliminated. Since no DFT is involved, there is no risk of spectral leakage due to the fundamental frequency deviation. The second approach does not require a spectral correction procedure; which is an advantage of this method.

The algorithms are verified both on simulated and field data obtained from three different EAF plants. The comparison with the digital realization of the IEC flickermeter shows that both of the methods give satisfactory estimations of the light flicker with low computational complexity.

In particular, for the first approach, which is the spectral decomposition based one for light flicker evaluation of electric arc furnaces, the following should be noted:

- The proposed approach gives good estimates of the instantaneous flicker sensation of the EAFs when compared with the digital realization of the IEC flickermeter. Hence the short term flicker severity, P_{st}, which is computed from the instantaneous flicker sensation is also estimated successfully. The proposed method is especially suitable to estimate the light flicker at the MV busbar of EAFs, if the short circuit MVA of the busbar is not high enough to keep the system frequency deviation inside a tolerable range. When a fixed FFT window (typically $200ms$ long) is used without any spectral correction, even a deviation of $0.01Hz$ causes significant error in interharmonic estimation and hence the flicker severity.

- The proposed method has low computational complexity. All computations are simple vector operations achieved on spectral samples of the FFT of the voltage waveform in the neighborhood of the fundamental frequency. In most of the power quality (PQ) analyzers, FFT of the voltage waveform is already obtained for harmonic analysis. Moreover, the same frequency resolution and the FFT size are used for the harmonic computation are as recommended in the IEC standard [16]. Therefore, computation of the flicker will not load an extra burden if FFT is already being used in a PQ analyzer.

- The use of a time window of 10 cycles as recommended in the IEC standard does not give good results when the fundamental frequency deviates, especially during the boring and melting phases of the EAF operation, where high currents are drawn from the busbar. This is because of the leakage effect of the FFT process when the window size is not an integer multiple of the fundamental period. Therefore a leakage correction process is employed in the proposed approach. This correction leads to very successful estimates of both the instantaneous flicker sensation, S, and the short term flicker severity, P_{st}. However, for this correction to be successful, an accurate estimation of the fundamental frequency is essential.

- Related to the previous item: Once the fundamental frequency is estimated, another method to correct the FFT leakage would be to adjust the window length and recompute the FFT; however, this will result in window sizes which are not integer multiples of 2^n, where n is a positive integer, and the efficiency of the FFT algorithm will be reduced. This problem can be solved by changing the sampling frequency of the device; however, this would require re-sampling the signal, which is not preferred for on-line computations. Sampling frequency can also be changed by applying interpolation on the already-sampled signal, but this will always contain some error of the original signal due to the interpolation procedure. The proposed method helps to avoid these problems.

- The proposed method provides a good understanding of the effect of frequency spectrum of the voltage on the flicker sensation of the human eye and the brain.

- In the proposed method, the existence of the fundamental frequency is considered without any harmonics. In case of harmonics existing in the spectrum, interharmonic frequencies around the existing harmonics should also be considered. For example, in the existence of the second harmonic, the voltage waveform will be given as

$$v(t) = [V sin(2\pi ft) + V_2 sin(2\pi 2ft)] \left\{ 1 + \frac{\Delta V}{2V} sin(2\pi f_f t) \right\} \tag{4.1}$$

where V_2 is the second harmonic amplitude. In this case, spectral components will appear not only at $f \pm f_f$, but also at $2f \pm f_f$, with amplitudes $(\Delta V)/4$ and $(\Delta V)V_2/4V$ respectively. The components at $2f \pm f_f$ will be negligible when $(\Delta V)V_2/4V$ ratio is negligible compared with $\Delta V/4$, which is usually the case. However, if it is known that the foregoing EAF voltage contains significant amount of the harmonics compared to the fundamental, then the effects of the harmonics should also be considered in the instantaneous flicker sensation computation in the summation given in (2.10) with appropriate coefficients.

In addition, the following should be noted about the second proposed approach, Kalman-filtering based approach for light flicker evaluation of electric arc furnaces :

- This proposed approach gives good estimates of the instantaneous flicker sensation when compared with the digital realization of the IEC flickermeter. Hence the short term flicker severity, P_{st}, which is computed from the instantaneous flicker sensation is also estimated successfully. The proposed method is especially suitable to estimate the light flicker at the MV busbar of EAFs, if the short circuit MVA of the busbar is not high enough to keep the system frequency deviation inside a tolerable range.

- The proposed method has low computational complexity. Only two types of Kalman filters with easy implementations are used and the flicker causing interharmonic frequencies are obtained. Moreover, the frequency resolution and the window size in the harmonic computation are used as recommended in the IEC standard [16].

- Arc furnace data is not stationary; therefore, time window of longer than 10 cycles would not be a good choice. All the results in the proposed method are obtained with $5Hz$ resolution, but it is possible to obtain a higher resolution by increasing the number of state variables.

- The proposed Kalman-filtering based method consists of two Kalman filters, which are an EKF and a LKF. Initially an EKF is used. The output of this filter gives the fundamental frequency and envelope of the voltage waveform. In second part of the proposed method, a twelve-state LKF is used to obtain the spectral amplitudes at the corresponding flicker frequencies of $0, 5, 10, \cdots, 25Hz$ using the voltage envelope. In fact, to obtain the spectral decomposition of the waveform, all these can also be done by using only a single Kalman filter. In the proposed flicker estimation method, the fundamental frequency is computed by the EKF. If it is not necessary to obtain the fundamental frequency, only by using one LKF, the spectral decomposition around the fundamental can be obtained. For this case, a 22-state LKF model is used to obtain the interharmonics around the fundamental. Equation (3.8) can be rewritten as given in

$$v(t) = Vcos(2\pi ft) + \sum_{i=1}^{N} \frac{\Delta V_i}{4} \{cos(2\pi(f + f_{fi})t + \phi_i) + cos(2\pi(f - f_{fi})t + \phi_i)\}. \tag{4.2}$$

As it is clearly observed from this equation that the effect of the modulation appear as interharmonics at beat frequencies which are $f \mp f_{fi}$ in the spectrum. For $5Hz$ frequency resolution case, to obtain the interharmonics around the fundamental, voltage waveform, $v(t)$, can be considered as the sum of eleven sinusoidal waveforms at frequencies $25, 30, \cdots, 70, 75Hz$. For each of these waveforms, two state variables of in-phase and quadrature-phase components are determined and a 22-state LKF model is obtained. The output of the LKF gives the spectral amplitudes at the interharmonics around the fundamental, directly. Although the matrix dimensions of the state equations are increased, the advantage of this approach is that in stead of using two types of Kalman filters, only a single LKF is enough to obtain the same result.

- Another advantage of the proposed algorithm is that the selection of exact window size is not so critical. When the fundamental frequency deviates from its nominal value, the constant window size causes a considerably significant error in DFT-based algorithms. The proposed algorithm results, on the other hand, are not affected that much by the window size change as it can be observed from Table 4.1. The results in Table 4.1 are obtained by simulating a voltage waveform with single sinusoidal flicker frequency as given in (2.1). In this voltage waveform, $\Delta V/V$ is 0.260 and f_f is $10Hz$, which gives unity S response with the proposed algorithm as it is given in Table 3.4. Sampling rate is chosen as $3200Hz$ and resolution rate is $5Hz$, which means that there should be 640 samples per window

Table 4.1: The Effect of Changing the Number of Samples per Window to Instantaneous Flicker Sensation, S

Number of Samples	S	Number of Samples	S
640	1		
635	0.99	645	0.99
630	0.99	650	0.98
625	0.98	655	0.98
620	0.98	660	0.97

when the fundamental frequency is exactly $50Hz$. Table 4.1 shows the S responses for different number of samples per window. The results show that the fundamental frequency deviation is not so critical for the proposed method. S is estimated as close as 97% to the actual S value, even if the window size is changed from 640 samples to 660 samples.

When the Kalman filtering based approach of this research work is compared with the first spectral decomposition based approach on flicker computation, several points should be emphasized:

- The Kalman filtering based approach does not suffer from fundamental frequency deviation and hence does not require the spectral correction procedure applied in the first spectral decomposition based approach. Moreover, the fundamental frequency is computed inherently in the first step of the algorithm. The method does not include any fundamental frequency detection algorithm such as zero cross detection explained in the first proposed method [7] for precise detection of the fundamental frequency. However, if it is necessary to compute the fundamental frequency exactly, only by determining fundamental frequency as a state variable in the EKF algorithm, it is possible to obtain it at an intermediate step of the algorithm.

- The Kalman filtering based approach uses 10 cycle windows for analysis. It is possible to reduce the window size for less stationary voltage signals, such as the case in EAF plants, without losing the frequency analysis resolution, at the expense of less accurate frequency estimates. However, in the DFT-based approach, reducing the window size means reducing the frequency resolution and hence the algorithm accuracy.

- The first method is faster than the second one. Therefore, a compromise should be made between the computation time and the accuracy of computation.

REFERENCES

[1] IEC 61000-4-15: "Testing and Measurement Techniques - Flickermeter - Functional and Design Specifications", 2002.

[2] C.J. Wu, Y.J. Chen, "A Novel Algorithm for Precise Voltage Flicker Calculation by Using Instantaneous Voltage Vector", IEEE Transactions on Power Delivery, vol. 21, no. 3, pp. 1541–1548, 2006.

[3] S.J. Huang, C.W. Lu, "Enhancement of Digital Equivalent Voltage Flicker Measurement via Continuous Wavelet Transform", IEEE Transactions on Power Delivery, vol. 19, no. 2, pp. 663–670, 2004.

[4] M.T. Chen, "Digital Algorithms for Measurement of Voltage Flicker", IEE Proceedings- Generation, Transmission and Distribution, vol. 144, no. 2, pp. 175–180, 1997.

[5] A. Hernandez, J.G. Mayordomo, R. Asensi, et.al, "A New Frequency Approach for Flicker Evaluation of Arc Furnaces", IEEE Transactions on Power Delivery, vol. 18, no. 2, pp. 631–638, 2003.

[6] C.J. Wu, T.H. Fu, "Effective Voltage Flicker Calculation Algorithm Using Indirect Demodulation Method", IEE Proceedings- Generation, Transmission and Distribution, vol. 150, issue 4, pp. 493–500, 2003.

[7] N. Kose, O. Salor, "New Spectral Decomposition Based Approach for Flicker Evaluation of Electric Arc Furnaces", IET Generation, Transmission, Distribution Journal, vol. 3, issue 4, pp. 393–411, 2009.

[8] C.W. Lu, S.J. Haung, C.L. Huang, "Flicker Characteristic Estimation of an AC Arc Furnace", Electric Power Systems Research, Elsevier, vol. 54, no. 2, pp. 121–130, 2000.

[9] T. Keppler, N.R. Watson, S. Chen, J. Arrilaga, "Digital flickermeter realisations in the time and frequency domains", Proceedings of Australasian Power Engineering Conference, Perth Australia, Sept. 2001.

[10] M. Gol, O. Salor, B. Alboyaci, B. Mutluer, I. Cadirci, M. Ermis, "A new field-data based EAF model for power quality studies", Proc. of the IEEE Industry Applications Society Annual Meeting, Canada, 2008.

[11] R. Thottungal, P. Anbalagan, T. Mohanaprakash, et.al., "Power System Stabilization in Multi Area System by Using HVDC Link", Academic Open Internet Journal (www.acadjournal.com), vol. 19, 2006.

[12] X.J. Jiang, Z.Y. Tang, Z.Y. Dong, T.K. Saha, "An Advanced Method for Eliminating Impacts from Frequency Deviations in Power System Signal

Processing", Electric Power Systems Research, Elsevier, vol. 67, no. 3, pp. 177–184, 2003.

[13] C.S. Chen, H.J. Chuang, C.T. Hu, S.M. Tseng, "Mitigation of Voltage Fluctuation for an Industrial Customer with Arc Furnace", Proceedings of IEEE Power Engineering Society Summer Meeting, vol. 3, pp. 1610–1615, 2001.

[14] V. Terzija, V. Stanojevic, "Robust Estimation Algorithm for Power Components Measurement", Proceedings of IEEE PES Power Systems Conference and Exposition, pp. 2229–2235, 2006.

[15] Y. Liu, "A US-Wide Power Systems Frequency Monitoring Network", Proceedings of IEEE PES Power Systems Conference and Exposition, pp. 159–166, 2006.

[16] IEC 61000-4-7: "Testing and Measurement Techniques - General Guide on Harmonics and Interharmonics Measurements and Instrumentation for Power Supply Systems and Equipment Connected Thereto", 2003.

[17] N. Kose, O. Salor, "A New Frequency Domain Approach for Light Flicker Evaluation of Power Systems", I2MTC 2009, International Instrumentation and Measurement Conference, Singapore, May 5-7 2009.

[18] N. Kose, O. Salor, K. Leblebicioglu, "Interharmonics Analysis of Power Signals with Fundamental Frequency Deviation Using Kalman Filtering ", submitted to Electric Power Systems Research, Elsevier, July 24 2009.

[19] N. Kose, O. Salor, K. Leblebicioglu, "A Kalman Filtering Based Approach for Light Flicker Evaluation of Power Systems", submitted to IET Generation, Distrubution and Transmission Journal, March 05 2009.

[20] J.A. Pomilio, S.M. Deckmann, "Flicker Produced by Harmonics Modulation", IEEE Transactions on Power Delivery, vol. 18, no. 2, pp. 387–392, 2003.

[21] T. Keppler, N.R. Watson, J. Arrilaga, S. Chen, "Theoretical Assessment of Light Flicker Caused by Sub- and Interharmonic Frequencies", IEEE Transactions on Power Delivery, vol. 18, no. 1, pp. 329–333, 2003.

[22] T. Demirci, A. Kalaycioglu, O. Salor, et. al., "National PQ Monitoing Network for Turkish Electricity Transmission System", Proceedings of Instrumentation and Measurement Technology Conference, Poland, May 1-3 2007.

[23] O. Salor, "Spectral Correction Based Method for Interharmonics Analysis of Power Signals with Fundamental Frequency Deviation", Electric Power Systems Research, Elsevier, vol. 79, pp. 1025–1031, 2009.

[24] M.B. Duric, Z.R. Durisic, "Frequency measurement in power networks in the presence of harmonics using Fourier and zero crossing technique", IEEE Proc. Power Tech., pp. 1–6, 2005.

[25] E. Ozdemirci, Y. Akkaya, B. Boyrazoglu, et. al., "Mobile Monitoring System to Take PQ Snapshots of Turkish Electricity Transmission System", Proceedings of Instrumentation and Measurement Technology Conference, Poland, May 1-3 2007.

[26] Güç Kalitesi Milli Projesi, http://www.guckalitesi.gen.tr, last visited on August 2009.

[27] G. Welch, G. Bishop, "An Introduction to the Kalman Filter" Technical Report, University of North Carolina at Chapel Hill, 2006

[28] A. Girgis, J. Stephens, E. Makram, "Measurement and Prediction of Voltage Flicker Magnitude and Frequency", IEEE Transactions on Power Delivery, vol. 10, no.3, 2005.

[29] G.W. Chang, C.I. Chen, Y.J. Liu, M.C. Wu, "Measuring power system harmonics and interharmonics by an improved fast Fourier transform-based algorithm", IET Generation, Transmission and Distribution Journal, vol. 2, no. 2, pp. 192–201, 2008.

APPENDIX A

IEC FLICKERMETER RESPONSE FOR RECTANGULAR FLUCTUATIONS

The IEC flickermeter response for rectangular fluctuations for $230V$ lamp and $50Hz$ system is given in Table A.1.

Table A.1: Normalized Flickermeter Response for Rectangular Voltage Fluctuations, 230V/50Hz system - IEC Standard 61000-4-15

Hz	Voltage Fluctuation %	Hz	Voltage Fluctuation %
0.5	0.514	10.0	0.205
1.0	0.471	10.5	0.213
1.5	0.432	11.0	0.223
2.0	0.401	11.5	0.234
2.5	0.374	12.0	0.246
3.0	0.355	13.0	0.275
3.5	0.345	14.0	0.308
4.0	0.333	15.0	0.344
4.5	0.316	16.0	0.376
5.0	0.293	17.0	0.413
5.5	0.269	18.0	0.452
6.0	0.249	19.0	0.498
6.5	0.231	20.0	0.546
7.0	0.217	21.0	0.586
7.5	0.207	22.0	0.604
8.0	0.201	23.0	0.680
8.8	0.199	24.0	0.743
9.5	0.200	33.3	1.670